Optimization of Coat-hanger Die Using 2-Way FSI and Adjoint Method

Clifford Omonini

Mechanical & Aerospace Engineering

Submitted in fulfilment of the requirements for the degree of Master of Science in Mechanical & Aerospace Engineering

NAZARBAYEV UNIVERSITY

School of Engineering and Digital Sciences
Department of Mechanical & Aerospace Engineering
Nazarbayev University

53 Kabanbay Batyr Avenue,
Nur-Sultan city, Kazakhstan, 010000

Supervisor: Asma Perveen
Co-supervisor: Dongming Wei

April 2024

DECLARATION

I hereby, declare that this manuscript, entitled "Optimization of Coat-hanger Die Using 2-Way FSI and Adjoint Method**"** is the result of my own work except for quotations and citations which have been duly acknowledged.

I also declare that, to the best of my knowledge and belief, it has not been previously or concurrently submitted, in whole or in part, for any other degree or diploma at Nazarbayev University or any other national or international institution.

Name: Clifford Omonini

Date: 22/04/2024

Abstract

The coat-hanger dies are extensively utilized in the plastic film and sheet extrusion sector. The product's quality and the extrusion machine's power requirements are contingent upon the flow uniformity at the die exit and the amount of pressure drop, respectively. Designing a die that can provide uniform flow at the die exit and minimize pressure drop is challenging for die manufacturers. This study investigated the die utilized by a local polypropylene sheet manufacturer. It enhanced the die's design regarding deflection at the exit, uniformity of outlet velocity, uniformity of shear rate at the walls, and pressure drop. This was achieved by employing Scheme Programming Language and the licensed CFD package, Ansys FLUENT Workbench 2020 R2, based on the finite element method. The rheological characteristics of the polypropylene were characterized using the Power law, Cross law, and Carreau-Yasuda viscosity model. The FSI analysis results indicate that by raising the die body thickness to 100mm and reducing the number of supports to 4, the deflection at the exit is reduced to 1.03%. Furthermore, the analysis of the simulation results acquired using the adjoint optimization method showed that the optimized die design outperforms all three aspects by ensuring uniform exit velocity, wall shear rates, and reduced pressure drop.

Acknowledgements

I want to express my most profound appreciation to my supervisor, Ass. Professor Asma Perveen, as well as to my principal investigator, Professor Dongming Wei, for the project titled "Design and Development of Multiphysics Algorithm for Polymer Sheet Processing Die Design SSH2021012," and to Professor Dichuan Zhang. The fact that I could complete this master's program is a direct result of their guidance and supervision throughout my academic pursuits. I want to thank them for the several hours of conversation they have provided me, particularly in fluid mechanics, materials engineering, structural engineering, and mathematics.

Table of Contents

List of Abbreviations and Symbols

CFD	Computational Fluid Dynamics
FSI	Fluid –Structure Interaction
FEA	Finite Element Analysis
FDM	Finite Difference Method
∇	Gradient operator
v	Velocity vector
P	Hydrostatic pressure
τ	Stress tensor
ρ	Material density
g	Acceleration due to gravity
γ	Shear rate
η	Apparent viscosity
k	Consistency index
n	Power-law index
μ_0	Zero shear viscosity
μ_∞	Infinite shear viscosity
$\boldsymbol{\lambda}$	Time constant
$\boldsymbol{T}$	Stress tensor
f	Body force
E	Young modulus
υ	Poisson's ratio
P_{is}	Melt pressure at the inner surface
v_t	Component of velocity which is tangential to the surface normal coordinate to the surface
P_0	Pressure acting externally at the die exit
h^I	N-minus-1 nodal 1/2-height parameters of the design
N	Overall number of design parameters
l_{exit}	Edge of the die outlet
L	Overall length along the edge of the die exit
v_a	Mean velocity at the die exit
$\bar{v}_p$	Required gap-wise mean velocity at the exit
Q	Flow rate
g_1, g_2, g_3	Constraints
$\boldsymbol{\lambda}$	Adjoint variable

List of Tables

List of Figures

List of Publications

1. Igali, Dastan, **Omonini Clifford**, Asma Perveen, Dichuan Zhang, and Dongming Wei. "Optimization of Non-Newtonian Flow through a Coat-Hanger Die Using the Adjoint Method." Designs 7, no. 6 (2023): 138.
2. Sharipkhan, Nurdaulet, **Omonini Clifford**, Asma Perveen, Dichuan Zhang, and Dongming Wei. "Investigation of Co-Extrusion Using a Coat Hanger Die with Different Feedblock Cross-Section." Key Engineering Materials 973 (2024): 131-137.
3. **Omonini Clifford**, Asma Perveen, Dongming Wei, and Dichuan Zhang Investigation of Coat-hanger Die Deflection: Fluid Structure Interaction for Different Material Laws and Support, (submitted).

Appendices

Chapter 1- Introduction/ Background of Study

1.1 General

The extrusion process is widely used in the polymer processing industry [1] and can produce a wide range of polymer-based materials [2] Coat-hanger dies play a crucial part in manufacturing many different items, including plastic films, sheets, pipes, melt-blown textiles, spun bond fabrics, and fibres [3].

Coat-hanger die extrusion is a watershed moment in the development of the polymer manufacturing industry. From thin films to intricate features, this method has proven indispensable in the plastics industry. When advances in polymer science and engineering enabled new production processes in the mid-twentieth century, this technology started to take form.

In the late nineteenth century, Alexander Parkes invented celluloid, a cellulose-based plastic, which marked the starting point of the extrusion technique as we know it today. In the mid-twentieth century, the coat-hanger die design was introduced, completely altering the extrusion procedure [4]. Demand for more precise regulation of extruded product dimensions, particularly in producing thin films and sheets, led to this development.

A die with a horizontal distribution manifold and vertical distribution channels is frequently known as a "coat-hanger die" because of its unique shape. The design improves the product's consistency and quality by allowing for a more uniform dispersion of polymer melt throughout the die. Coat-hanger dies have been used to enhance the extrusion procedure since at least the beginning of the twentieth century, when scientists and engineers first experimented with them.

The second part of the 20th century saw major advancements in coat-hanger die design. Researchers focused on optimizing die shape, material selection, and extrusion process parameters. The coat-hanger die design's versatility and dependability led to its widespread use in sectors such as packaging, construction, and automotive.

Coat-hanger die manufacturing increased between the 1970s and 1980s due to computer-aided design and simulation approaches. Engineers can now predict and monitor polymer melt flow inside the die, resulting in more precise designs and improved performance. Computer tools also improved the extrusion process by requiring minimal redos via trial-and-error methods.

The number of polymers suitable for coat-hanger die extrusion has increased as polymer investigation has advanced. Coat-hanger dies were intended for conventional polymers such as polyethylene and polypropylene. However, they are now widely utilized for sophisticated plastics and elastomers. Manufacturers modified the coat-hanger die design to meet the growing need for diverse, bespoke polymer items.

Nowadays, coat-hanger dies are essential in producing plastic films, sheets, and profiles, among other contemporary items [5]. Their accuracy in controlling melt width and thickness makes them essential in industries that value constant product quality. In addition, the coat-hanger die's adaptability to diverse polymer compositions benefits the ecosystem by reducing waste.

Extrusion using coat-hanger dies has a long history of innovation and evolution. The coat-hanger die has left an indelible effect on the polymer processing landscape, from its humble origins in the mid-twentieth century to its widespread use in various sectors today. Further advancements and uses of this die design are expected to shape the future of polymer extrusion as technology improves.

The design of coat-hanger dies has always been governed by two critical considerations: achieving a consistent velocity at the exit point and a minimal pressure loss [3]. According to Han and Wang [6], disrupting this equilibrium might have harmful consequences. pressure drops of this scale contribute to greater energy consumption and increase the risk of die plate separation. Non-uniform velocities at the exit may result in an undesired thickness of the product.

Die deflection has received little attention in the scientific literature, even though managing internal pressure inside the melt flow is recognized to be critical [7], [8]. Research must be conducted into how increased internal melt pressure affects die deflection and velocity uniformity at the die exit. Due to this lack of information, determining how much pressure is needed to improve flow uniformity while reducing the risk of die deflection is critical [9].

As computing power has increased, optimization methods have become increasingly integral to modern die design procedures. The robust instrument of computational fluid dynamics (CFD) is now an integral part of the optimization tactics used in the manufacturing sectors. Automatic modelling methods used in die design are based on advanced solution strategies with origins in CFD [10], [11]. Increases in computational power have revolutionized die design by allowing for finer-grained optimization.

The adjoint method stands out among these optimization strategies as an accessible and effective choice for enhancing coat-hanger dies. Using the rising computer capability, the adjoint technique guides users through the complex interplay of factors during the extrusion process. The optimization process stands to gain efficiency and precision with the implementation of this technology. Figure 1.1 shows the fluid and solid geometry of the coat-hanger die used in this study.

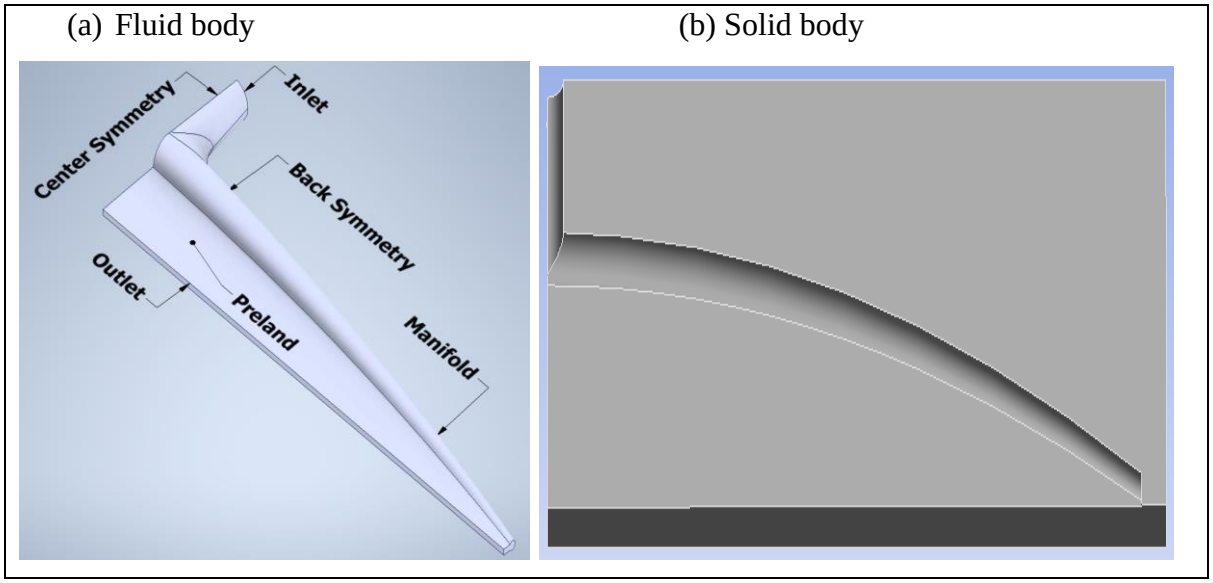

Figure 1.1 Coat-hanger Die (a) Fluid body (b) Solid Body [6] [13]

1.2 Research problems

The following research gaps were identified after reviewing various studies on the design of coat-hanger dies for extrusion.

a) Although many reports of the CFD studies of coat-hanger die, only few studies have considered the die-body deflection at the exit.

b) The literature uses many optimization techniques to optimize the fluid body of the coat-hanger die for optimal performance with a uniform velocity distribution at the exit and low-pressure drop. However, only a limited CFD report uses the adjoint method for die body optimization.

1.3 Aims and Objectives

This research has developed mathematical models and optimization methodologies for coat-hanger die design based on past studies. The latest is the adjoint approach for coat-hanger die optimization, which will be published soon.

This research study will analyze the flow distribution within the die, which can cause die body deflection. The material law, die body thickness, and pressure, which can influence lower deflection, would be used to further optimize the die's shape using the adjoint method to have lower pressure drop and enhanced velocity uniformity at the die exit.

.

The specific objectives of this study include.

- Study the die deflection using 2-Way-FSI to determine the optimal die support and thickness which will become the base design for further improvement.
- Compare the rheology effect on pressure, velocity distribution and die deflection.
- Minimize mass flow variance to enhance uniform velocity distribution at the die outlet and reduce pressure loss between the inlet and outlets of the die.
- Compare the residence time distribution for various rheology and die designs.

Chapter 2 – Literature Review

2.1 Extrusion

By forcing a melted polymer through a die with a hole, extrusion is a way to make continuous products with a uniform cross-section, like rods, sheets, pipes, films, and wire insulation covering [12]. As shown in Figure 2.1, polymer pellets are fed into an extruder using a hopper during molding. It is then moved by a feeding screw and forced through a die, turning it into a continuous polymer product [13]. The heated elements above the barrel soften and melt the polymer. Using thermocouples, one can control the temperature of a material. Following its release from the die, the product is either cooled by airflow or submerged in water [1]. Unlike metals, extrusion is a constant process for polymers that goes on as long as raw pellets are available. Thermoplastics are usually processed with extrusion, but elastomers and thermosets can also be processed this way.

This situation involves cross-linking in the extruder while it is heated and melting. Products made from extruded thermoplastic can be shaped even more using the thermoforming method.

A thermoplastic extruder consists of a tubular barrel, typically heated by electricity, along with a rotating screw, ram, or plunger inside the barrel. At one end, there is a hopper where the material to be extruded is fed into the screw, ram, or plunger. At the other end, a die shapes the extruded mass [14].

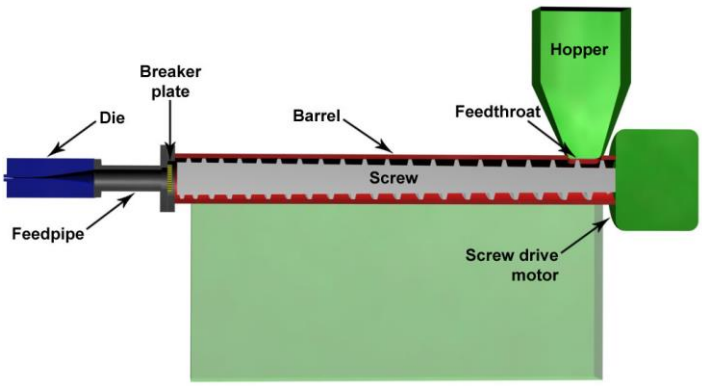

Figure 2.1: Outline of the Extrusion Process [1]

2.1.1 Extrusion Process

During plastic extrusion, the initial material is often in the shape of tiny beads known as nurdles (sometimes referred to as resin). These nurdles are fed into the extruder barrel from a hopper on top, using the force of gravity. Colorants and UV inhibitors, in either liquid or pellet form, are commonly used as resin additives. These additives can be blended with the resin before it reaches the hopper. The technique shares many similarities with plastic injection molding in terms of extruder technology; however, it often varies and is a continuous process [1].

The material contacts the screw after being fed into the barrel through the feed throat, which is situated toward the back of the barrel. The plastic beads are hurled in the direction of the heated barrel by a screw that rotates at a rate of generally 120 rpm. Because of things like viscous heating and other variables, the temperature at which extrusion is intended to occur is frequently differs from the temperature established for the barrel [15]. In most cases, a heating profile is devised for the barrel, and it involves the use of at least 3 distinct PID-controlled heater zones. These zones cooperate to gradually increase the barrel's temperature, beginning at the back (which is where the plastic goes in) and moving toward the front of the barrel. Because of this, the plastic beads can gradually melt as they are propelled down the barrel. As a result, there is a decreased risk of the barrel overheating, which could lead to polymer degradation [16].

The intense pressure and the constant rubbing against one another that takes place inside the barrel both contribute to the added heat. When an extrusion line operates at a sufficiently high speed, it is possible to turn off the heaters and rely entirely on the pressure and friction within the barrel to keep the melt temperature at the required level. Cooling fans are typically incorporated into the design of most extruders to manage the temperature by removing excess heat and ensuring that it remains below a specific limit. Cast-in cooling jackets are applied when forced air cooling is insufficient to achieve the desired temperature.

The plastic that has been melted emerges from the screw at the front of the barrel and travels through a screen pack, which removes any contaminants that may be present in the molten substance. Due to the possible pressure in this place which could be more than 5,000 psi (34 MPa), the screens have been strengthened with a breaker plate [16]. A *breaker plate* is a solid metal disk that has many perforations. The combination of the breaker plate and the

screen pack serves an additional purpose: generating counter pressure inside the barrel. Back pressure must be there for any chance of the polymer melting evenly and effectively blending. The amount of pressure generated can be altered by changing the components that make up the screen pack. These components include the number of screens, the significance of the wire weave on the screens, and any other relevant attributes. The phenomena known as "rotational memory" in molten plastic is eliminated because of the combination of this breaker plate and screen pack. A phenomenon known as "longitudinal memory" is created in its place.

The melted plastic goes through the breaker plate and then into the die. The die is what shapes the product, and it needs to be made so that the molten plastic flows smoothly from a cylindrical shape to the shape of the product. At this point, uneven flow can leave the product with unwanted residual stresses at some places in the profile, which can cause it to warp when it cools. You can make many different forms, but they can only be continuous profiles.

The item needs to be cooled, generally done by running the extrudate through a water bath. Plastics are very good at keeping heat in, so it is hard to cool them down quickly. Plastic loses its heat 2,000 times more slowly than steel does. In a line for extruding tubes or pipes, a vacuum is carefully managed and acts on a sealed water bath to keep the still-molten tubes or pipes from collapsing. Cooling is done for things like plastic sheets by pulling them through a set of cooling rolls. Air cooling can work well as the first step in cooling films and fragile sheets, like in blown film casting.

Plastic extruders are often used to clean, sort, and blend recycled plastic trash or other raw materials before reusing them. This material is usually extruded into strands that can be chopped into bead or pellet stock and used as a starting point for further processing.

The melted plastic moves into the die after going through the breaker plate and making sure that the molten plastic changes evenly from a cylinder shape to the desired profile shape of the product is what the die does to give the product its end shape. If the flow is not smooth at this point, the product might have unwanted leftover stresses in some places along the profile, which can cause it to deform after it cools.

The item is usually cooled down in a water bath. Plastics are very good at keeping heat in, making them hard to cool down quickly.

Plastic doesn't conduct heat as well as steel does—2,000 times less well. In a tube or pipe extrusion line, a vacuum is carefully controlled over a tightly sealed water bath to keep the newly made tube or pipe from collapsing while it is still liquid. Plastic sheets and similar things are cooled by running them through a set of cooling rolls. Air cooling can work well as the first step in chilling films and fragile sheets, like in the process of blown film casting.

Plastic extruders are often used to handle recycled plastic waste or other raw materials that have been cleaned, sorted, and mixed. This material is often pushed through a machine to make threads that can be cut into small pieces and used as starting materials for more work.

2.1.2 Extrusion Materials

When heat is applied, thermosets can be extruded, but thermoplastics are the most common type of plastic that can be extruded. This group includes a wide range of high-performance, engineering-grade, and everyday plastics. All of them can have either amorphous or rigid molecular structures.

Extruding high-performance plastics is expensive and not often done. These plastics are made for extreme conditions and have great temperature and mechanical properties. Polyetherketone (PEK) is a type of plastic used in aircraft and cars because it doesn't tear easily or react with chemicals. Besides that, it stays strong in many different temperatures.

The next level down is engineering plastics, special plastics made to have unique properties while still being less expensive than high-performance materials. Some of the products are TPE, ABS, nylon, and polycarbonate. Most extrusions are made of commodity plastics, flexible materials that can be used for many things. Polypropylene, polyethylene, and PVC are the plastics that are the best value for money.

The plastics in these three groups can have an amorphous or rigid polymer structure, determining how they work. Amorphous structures, like those in PVC, ABS, and polycarbonate, have disorganized and bendable polymer chains. Because of these qualities, they are flexible, springy, and resistant to being hit or shrunk. Despite this, they are not as strong or resistant to chemicals as rigid-structure plastics like HDPE or polypropylene. These plastics have hard structures that make them strong, stiff, and heat resistant. However, they tend to get smaller and are not very resistant to being hit.

2.2 Polymers

The word "polymer" comes from the Greek language and means "many parts" [17]. As shown in Figure 2.2, polymers are made up of molecules that can organize themselves into long chains of smaller recurrent units. Examples of polymers include plastics and rubber.

Figure 2.2: illustration of a polymer chain in schematic form.

Polymers differ based on the chemical and physical features of the unit that repeat itself in the chains. Plastics are made of polymers that have been mixed with different substances before being used to make many things we use every day. Rubber is made of plastics that can be bent and shaped in many ways. "Plastics" usually refer to things that do not break down naturally and pollute the seas and landfills significantly [17]. Even though plastics can be recycled in large amounts, the collection, sorting, and recycling programs in each country are very different. Plastics are known for having

- low strength and stiffness
- Maximum temperatures that they cannot handle.
- Plastics continuously change shape, called "creep," when a force is applied [18].

The above features are not as good as common materials like metal, wood, or clay. Figure 2.3 shows that since 1989, the volume of plastics used has always been higher than that of steel. In addition, this gap keeps getting bigger.

.

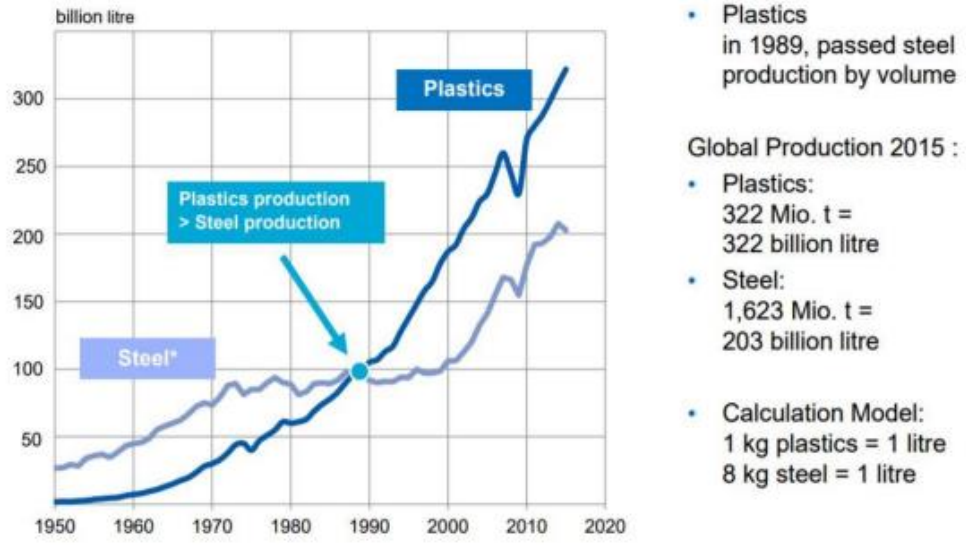

Figure 2.3: Comparison of plastic and steel consumption volumes (source: PlasticsEurope)

The demand for plastics keeps getting higher for the following reasons

- Cost-effective and easy to shape into complex forms with little processing and finishing needed.
- Having low densities, which lets them be used to make lightweight but long-lasting things.
- Making fibers, sheets, tubes, and profiles is easy.
- They keep heat and electricity from moving.

They also have unique qualities like being flexible, evident in some cases, long-lasting without noticeable wear and tear, not letting gases and liquids through in some polymer grades, being biocompatible for medical implants and devices, and being able to be combined with glass fibers, natural fibers, carbon fibers, carbon nanotubes, or graphene to make solid materials.

2.3 Polymer Melts

Depending on the rate of flow or deflection, polymer melts can exhibit either a viscous or elastic behavior. Since film-blowing lines now work at significantly greater draw speeds, a material that ran smoothly on a line 20 years ago may not run at all on a line today. New circumstances may have had unfavourable consequences on processibility of the material while drastically reducing the processing time. Another instance is when the injection molding

process fails to produce optimal results because of alterations to the material's chemistry, the length of the process, or both. Orientation effects can be induced by them, leading to unwanted anisotropy in the mechanical characteristics of the final products. Understanding and quantifying a polymer's viscous and elastic qualities is the goal of polymer melt rheology, which is used to ensure that the process parameters are in harmony with the material's melt properties.

2.4 Dies

When extruding polymers into various shapes and forms like sheets, tubes, and films, dies play a critical role. The extrusion method involves melting raw polymer material and forcing it through a die to form a continuous shape. The die gives the extruded polymer its final shape [20].

The die's fundamental function is to shape the molten polymer into the appropriate form. It functions as a mold, imparting its shape and dimensions to the extruded material.

2.5 Literature Review on Optimization Techniques for Manifold Dies

Coat-hanger dies are essential components when extruding polymer materials into flat, uniform sheets. Optimizing the performance of the coat-hanger dies is crucial to achieving accurate thickness control and consistent distribution of the extruded material. Coat-hanger dies are optimized in several ways to increase productivity and consistency, resulting in uniformly high-quality sheets. These methods maximize product quality and manufacturing efficiency by optimizing various factors, including die design, material choice, temperature management, and process parameters.

Matsubara [22] determined a vital design parameter (the radius variation throughout the entire manifold length) for coat-hanger dies by solving the analytical equations for flow modeling. This parameter maintains both the width-dependent flow rate and residence duration. Matsubara [23] also applied this technique to T-dies. Using a single objective function, they attempted to solve the optimization problem of creating manifold die. The optimization procedures used empirical methods, regression analysis, sequential quadratic programming, gradient methods, and evolutionary algorithms.

Winter and Fritz [24] advocated adopting a particular design process for a coat-hanger die. Regardless of the flow rate or polymer viscosity, this approach considers the consistency of the exit velocity and average residence duration. It also considers flow separation. The die's geometry was determined to be that of a square and circular manifold with a constant thickness along the parallel section. The length of the manifold determined the width or diameter, while the height of the parallel portion was a design variable.

To avoid dead spots in the transition to the parallel zone, Liu et al. [25] developed a method to improve the efficiency of coat-hanger dies with a non-circular manifold. The goal was to pinpoint the manifold and parallel zone geometries that guarantee a constant flow pattern and residence period regardless of the polymer or operation conditions. The results of the solutions were evaluated with the help of computational modeling software. A coat-hanger dies with a linearly tapered inner cavity and a straight outer cavity was created by Lee and Liu [26] using a similar heuristic technique. However, they examined the influences of inertia, gravity, and viscosity. Following this, Liu et al. [27] and Yu and Liu implemented a unified lubrication approximation to model the flow of polymers inside the die, respectively, to create a coat-hanger die [27] and a tapering coat-hanger die.

Na and Kim [28] used an empirical method to design coat-hanger dies with a circular manifold and a linear taper. The goal was to obtain a constant flow rate spread across the die's transverse outlet. This was achieved by using a 3-dimensional FEM modeling code to consider the slot thickness, manifold angle, and land length. More recently, Huang et al. [29] used a simple empirical approach to create dies for coat-hangers. The goal was to maximize the consistency of outlet velocities from the die. The slit's height, together with the manifold's radius and angle, were considered.

More methodical optimization strategies were developed with the help of regression procedures like Taguchi methods. Researchers Chen et al. [30] investigated how material rheology, gap thickness, manifold angle, and flow velocity affected the thickness consistency of coat-hanger dies. The Taguchi method was used to find the best proportions for dies of varied widths. An analytical model was used to evaluate the solutions' efficacy; the flow rate was included as a design variable.

Recently, a response surface method was used by Razeghiyadaki et al. [31], [32] to determine the ideal coat-hanger die profile. The objective was to achieve a consistent velocity

at the die lips. The response surface was computed using commercially available software; the parameters for the computations were determined via a centralized composite design of experiments (DOE). Five parameters, including the die's depth and width and the locations of three nodes along the spline, were used to define the spline curve that was used to outline the geometry. To optimize, they located the minimum value of the resulting quadratic function.

A global RSM with Kriging interpolation and Sequential Quadratic Programming (SQP) was used by Lebaal et al. [33] to calculate the coat-hanger die geometry. The goal was to reduce the deviation from the mean velocity of the exiting die. Considering the pressure needed by the flow as a limitation, the flow distribution channel's depth was evaluated as the choice variable. After that, three factors—the width of the gap, the height of the relaxation zone, and the depth of the channel repartition—were considered in making a final call [34]. The size of the distribution channel and the operation conditions could be calculated using the same method [35], and a similar flow equilibrium concept was also employed to create a wire coat-hanger [36]. To use the sequential quadratic programming (SQP) technique, the objective function and constraints must be of second-order differentiability. This need was satisfied here because the goal function and constraints had already been set via regression.

Table 2.1 shows a summary of the literature reports done so far on the optimization of the coat-hanger die for uniform velocity distribution at the exit and low-pressure drop.

Table 2.1 : Literature reported on coat-hanger dies.

S\No.	Reference	Year	Findings	Limitations/research gap
1	[37]	2007	Reduction in pressure drop which enhanced the velocity distribution at the die exit at less computational time.	• Unable to combine the pressure drop and mass flux variance. • Unable to study the effect of pressure on the die deflection.
2	[38]	2011	• As the manifold angle, land height, and slot spacing were increased, the coefficient of	• Was unable to study the pressure drop. • The effect of the pressure on die

			variation at the die outlet was greatly reduced. • Die land has minimal effect on residence time.	deflection was also not considered.
3	[10]	2020	• Derived an equation for designing a coat-hanger die. • Discovered that the uniformity of velocity at the die exit is affected by the extrusion material. • Greater deflection is noted when a material other than the one utilized in the original die design is employed.	• Was unable to use any optimization technique to enhance the velocity uniformity at the die exit. • Only considered 1-Way-Fluid-Structure-Interaction.
4	[39]	2018	The pressure drop in the die was reduced when the adjoint was coupled together with FSI.	Only applied this to a duct.
5	[40]	2020	The combination of the Response Surface Method and Computational Fluid Dynamics produced a 20% improvement in the velocity distribution at the die outlet.	• Was unable to perform FSI. • Was unable to consider pressure drop.

Chapter 3 – Methodology

3.0 General

This section outlines the optimization process employed for the coat-hanger die. Initially, a 2-way fluid-structure interaction (FSI) analysis will be conducted to ascertain the optimal thickness and supports that minimizes deflection in the die. This analysis will be based on different rheological models. Subsequently, an adjoint optimization process will be performed utilizing the adjoint solver within the Ansys software. The utilization of the quarter fluid domain of the coat-hanger die is demonstrated in Figure 1. To optimize computational efficiency, limiting the analysis to only one-quarter of the fluid domain is possible, as the coat-hanger die geometry exhibits symmetric characteristics.

Ansys's static structural state tool, fluent, and system coupling capabilities will be utilized to establish a coupling between the Fluid and solid domains. Figure 2 is a flowchart that illustrates the 2-way Fluid-Structure Interaction (FSI) process. The equations that regulate the fluid and solid domains, as well as the deflection within the solid domain, are presented herein.

3.1. CFD Simulations

3.1.1. Geometric Model

The primary focus of this study pertains to the internal geometry of the die, as it plays a crucial role in determining the behavior of the fluid body as it flows through the channels of the die. This die is specifically engineered to facilitate the extrusion process of sheets with a width of 720 mm and a thickness of 3 mm. The morphologies of the fluid body within the die are seen in Figure 1.1.

3.1.2 Governing Equations

The underlying assumptions of the dynamic flow analysis about the polymer melt passing through a sheeting die are as follows:

- The polymer melt can be characterized as an incompressible non-Newtonian fluid.
- The flow of the polymer melt exhibits a steady state, isothermal, and fully-developed flow.
- A no-slip condition is assumed to exist between the die wall and the polymer melt.

Based on the aforementioned assumptions, the mathematical model utilized in this study will incorporate continuity and momentum conservation equations.

Considering a mass balance and momentum flux balance on a small control volume Δx.Δy.Δz in a space, we obtain [21], [31];

$$\nabla \cdot v = 0 \tag{3.1.1}$$

$$\rho v \cdot \nabla v = -\nabla P + \nabla \cdot \tau + \rho g \tag{3.1.2}$$

where ∇ is the gradient operator, v is the velocity vector, P is the hydrostatic pressure, τ is the stress tensor, ρ is the material density, and g is the acceleration due to gravity. The equation that describes the relationship between the constitutive properties and the viscosity function is given by:

$$\tau = \eta\dot{\gamma} \tag{3.1.3}$$

where $\dot{\gamma}$ is the shear rate and η is the apparent viscosity.

3.1.5 Rheology Models and Parameters

This research has adopted three rheology models: the power-law model, the Cross model, and the Carreau-Yasuda model [32].

3.1.5.1 Power law

$$\eta = k \,.\, \dot{\gamma}^{n} \tag{3.1.4}$$

3.1.5.2 Cross Model

$$\eta = \mu_{\infty} + \frac{\mu_0 - \mu_{\infty}}{1 + \lambda^{m}\gamma^{m}} \tag{3.1.5}$$

3.1.5.3 Carreau-Yasuda Model

$$\eta = \mu_{\infty} + (\mu_0 - \mu_{\infty})(1 + \lambda^2\gamma^2)^{\frac{n-1}{2}} \tag{3.1.6}$$

where K is consistency index (Pa s^n), n is power-law index, μ_0 is zero shear viscosity (Pa s), μ_{∞} is infinite shear viscosity (Pa s), $\dot{\gamma}$ is shear rate and λ time constant (s).

These models and their corresponding parameters are described in Table 3.1.

Table 3.1: Rheology models and parameters

Rheology Model	**Parameters**
Power law model	K = 8125 Pa s^n, n = 0.38
Cross model	μ_0 = 564.4 Pa s, μ_∞ = 0, λ = 0.017 s, m = 0.749
Carreau-Yasuda model	μ_0 = 1326 Pa s, μ_∞ = 0, λ = 0.12 s, n = 0.35

3.1.6. Boundary Conditions

In this research endeavor, one-quarter of the die will be utilized throughout all simulations to mitigate simulation duration effectively. At the inlet, the flow is assumed to be fully developed, with a volumetric flow rate ofof $8 \times 10^{-5}\ m^3/s$. The application of a no-slip boundary condition, also known as wall adhesion, is observed on the wall. Consequently, the velocities parallel and perpendicular to the wall were initialized to zero. The boundary conditions of zero average velocity and zero shear rates were imposed along the symmetrical planes. The boundary conditions at the exit were ultimately specified as having zero normal and tangential forces.

3.2 Die Deflection Analysis

Since we are assuming fully developed flow at the inlet and exit of the die [41],

$$\frac{\partial U}{\partial x} = 0\ also, V = W = 0 \tag{3.2.1}$$

where *x* is the direction of melt flow during extrusion.

Also, for the no-slip boundary condition: $\boldsymbol{V} = 0$ (3.2.2)

These equations can easily be solved using any of the finite element simulation algorithms.

For us to be able to determine the deflection of the die body, there is a need to solve 3-D stress-strain equations given as follows

From momentum equation

$$\nabla.\tau = \rho V.\nabla V \tag{3.2.3}$$

$$\tau = -PI + \mu(\gamma)(\nabla V \dot{+} \nabla V^T) \tag{3.2.4}$$

$$\nabla.\boldsymbol{T} - \boldsymbol{f} = 0 \tag{3.2.5}$$

where $\boldsymbol{T}$ is the stress tensor and f is the body force

If we express $\boldsymbol{T}$ components in Cartesian form, we have

$$T_{ii} = \alpha\left[(1-\upsilon)\frac{\partial u}{\partial x} + \upsilon\frac{\partial v}{\partial y} + \upsilon\frac{\partial w}{\partial z}\right], \tag{3.2.6}$$

$$T_{ij} = T_{ji} = \alpha\left(\frac{1}{2} - \upsilon\right)\left(\frac{\partial v}{\partial y} + \frac{\partial v}{\partial x}\right), \tag{3.2.7}$$

$$T_{jj} = \alpha\left[\upsilon\frac{\partial u}{\partial x} + (1-\upsilon)\frac{\partial v}{\partial y} + \upsilon\frac{\partial w}{\partial z}\right], \tag{3.2.8}$$

$$T_{jk} = \boldsymbol{T}_{kj} = \alpha\left(\frac{1}{2} - \upsilon\right)\left(\frac{\partial v}{\partial z} + \frac{\partial w}{\partial y}\right), \tag{3.2.9}$$

$$T_{kk} = \alpha\left[\upsilon\frac{\partial u}{\partial x} + \upsilon\frac{\partial v}{\partial y} + (1-\upsilon)\frac{\partial w}{\partial z}\right], \tag{3.2.10}$$

$$T_{ki} = T_{ik} = \alpha\left(\frac{1}{2} - \upsilon\right)\left(\frac{\partial u}{\partial z} + \frac{\partial w}{\partial x}\right), \tag{3.2.11}$$

The displacement vector can be expressed as $\boldsymbol{d} = ui + vj + wk$ (3.2.12)

$$\alpha = \frac{E}{(1+2\upsilon)(1-2\upsilon)}. \tag{3.2.13}$$

where E is the Young modulus and υ is Poisson's ratio

When analyzing the die exit deflection, the body force is taken as 0 since we assume that no external force is acting on it [41].

For us to solve equation 3.2.5 for the deflection across the entire region of the die body, the boundary conditions must be satisfied.

The polymer melt causes normal stress to act on the inner surface of the die body and this is expressed as follows

$$\boldsymbol{T}:nn|_{is} = -\tau:nn|_{is}, \tag{3.2.14}$$

where *n* is a unit vector which is normal to the inner surface of the die body.

$$\boldsymbol{T}:nn|_{is} = P_{is}, \tag{3.2.15}$$

Where P_{is} is the melt pressure at the inner surface.

The polymer melt also imposes a shear stress on the inner surface of the die body which is expressed as

$$\boldsymbol{T}:nt_{is} = -\tau:nt_{is}, \tag{3.2.16}$$

where **t** is a unit tangential vector to the inner surface of the die body.

If we substitute eqns. 3.1.2, 3.1.3 and 3.2.5, we have the following:

$$\boldsymbol{T}:nt_{is} = \mu\frac{\partial v_t}{\partial n}|_{is}, \tag{3.2.17}$$

where v_t is the component of velocity which is tangential to the surface and **n** is the normal coordinate to the surface.

The normal stress acting on the entire outside body of the die is given as follows;

$$\boldsymbol{T}:nn|_{os} = P_0, \tag{3.2.18}$$

where P_0 is the pressure acting externally at the die exit.

Therefore, the shear stress acting externally all over the surface of the die body in inviscid or stagnant air is given as follows

$$\boldsymbol{T}:nn|_{os} = 0. \tag{3.2.19}$$

3.2.1 Flow Chart for 2-WAY-FSI

Figure 3.1 shows the flow chart for the 2-way-fsi. The fluid solution is obtained using the Ansys fluent, which is then coupled with the solid domain setup in Ansys static structural using the Ansys system coupling. The number of iterations is set, and the simulation is allowed to run until convergence. The solution obtained will determine whether further iterations are needed.

Two domains will be considered in the FSI simulation, as shown in Figure 1.1: the solid body and the fluid domain. The solid body used in the FSI is assumed to comprise of Tool Steel with a density of 8000 kg m-3, Poisson's ratio of 0.29, Young modulus of 2.09 x 1011 Pa, and tensile yield strength of 1.03 x 109 Pa [42].

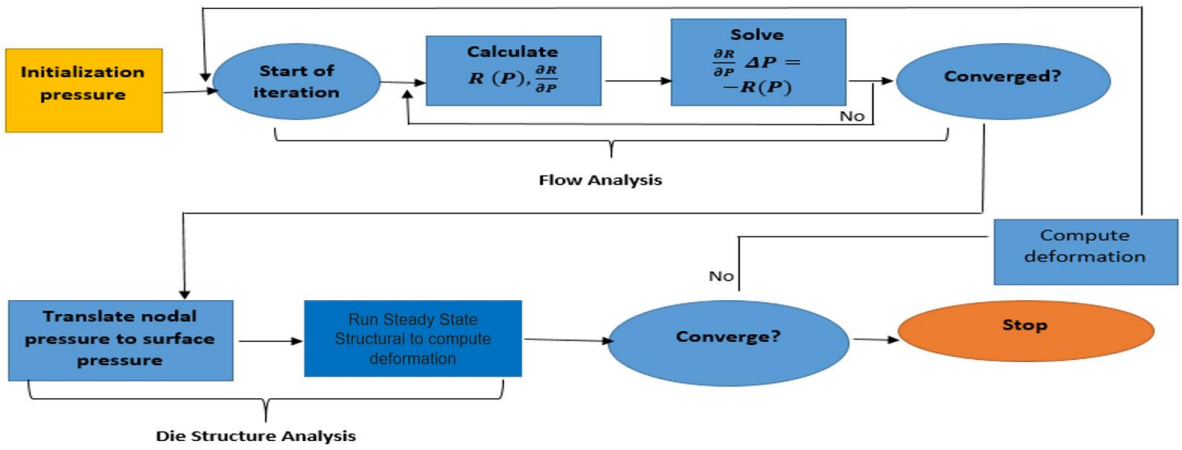

Figure 3.1: Flow Chart for 2-Way-FSI

3.3 Adjoint Formulation

The flowchart for the optimization process using the Adjoint method is shown in Figure 3.1.

Before executing the Adjoint solver, a forward simulation is necessary to obtain the starting Pressure and velocity values throughout the die body. The polypropylene's rheology will be defined using the Carreau-Yasuda viscosity model [43].

3.3.1 Adjoint-Based Optimization

Adjoint-based optimization has been known to work well for problems with many design factors [44]. It is based on the Adjoint method, making it possible to calculate sensitivities accurately. Sensitivities are calculated by finding the derivative of the objective function concerning the design parameters. No matter how many design variables there are, the amount of work that must be done on the computer stays the same because just one solution is needed for the adjacent counterparts of the governing equation system, the Navier-Stokes equations. Sensitivity analysis can be used on either a surface mesh or a volume mesh of the part that needs to be optimized to get information like uniform velocity and pressure drop [44].

3.3.2 Design Sensitivity Analysis (DSA)

Gradient-based optimization methods use design sensitivity to quickly find better designs. The design variables are factors like the ½ height of the die cavity or the input pressure variables. The system's performance metrics are things like f,g_1, g_2 , and ${g_3}^k$ in Eq. 3.3.1. Design sensitivities [44] measure these things. Models for the design sensitivities were made and the FEA was used to test them in the same way that the flow solution was tested. This way of analyzing avoids the mistakes and errors that come with FDM.

The adjoint method, which it is based on, makes it possible to calculate sensitivities accurately. Sensitivities are calculated by finding the derivative of the objective function around the design parameters. It does not matter how many design factors there are; the computing work stays the same because it only needs to solve the adjoint equivalents of the governing equation system, which are the Navier-Stokes equations. Sensitivity analysis can get information about things like consistent velocity and pressure drop. A surface mesh or a volume mesh of the area that needs improvement can be used for this study.

3.3.3 DSA for Coat-hanger Die.

This study investigates how pressure drop and die exit velocity variation affect die design quality. Pressure drop determines the dimensions of the extruder and the required power, while outlet velocity fluctuation influences the thickness uniformity of the sheet [45]. Mathematically, die design optimization is.

$$\min(J \epsilon \mathcal{R}^N) \qquad f(\phi) = P_{in}, \tag{3.3.1}$$

$$\text{Such that } g_1(\phi) = \frac{1}{L}\int(\frac{\bar{v}\,(\phi)}{v_a(\phi)} - 1)^2 dx \leq \varepsilon_1, \tag{3.3.2}$$

Eqn. 3.3.2 is integrated from the edge of the die exit (l_{exit}).

$$g_2(\phi) = (\frac{v_a\,(\phi)}{\bar{v}_p(\phi)} - 1)^2 \leq \varepsilon_2, \tag{3.3.3}$$

$${g_3}^k(\phi) = \frac{\|\nabla h^k(\phi)\|}{\|\nabla h_p\|} - 1 \leq 0, \tag{3.3.4}$$

This nonlinear restricted optimization aims to reduce the inlet pressures P_{in} as much as possible. Design variables are written as ϕ= {Pin, h^I}, I= 1, 2 ... N - 1, whereby h^I are the N-

minus-1 nodal 1/2-height parameters of the design and *N* is the overall number of design parameters [45].

The constraint g_1 in Equation 3.3.2 assesses variations in outflow velocity and ensures that the outlet velocity remains stable within the specified range [45]. This constraint maintains tight proximity between the mean gap-wise velocity at the outlet $\bar{v}(\phi)$, which is perpendicular to the die outlet in Figure 1.1, and the required average gap-wise exit velocity which is perpendicular to the die outlet in Figure 1.1, and the required average gap-wise exit velocity $v_a(\phi)$.

$$v_a(\phi) = \frac{1}{L}\int_{l_{exit}} \bar{v}\, dx, \tag{3.3.5}$$

where l_{exit} is the edge of the die outlet, and the overall length along the edge of the die exit is *L*. If g_1 is 0, it means that the calculated $\bar{v}(\phi)$ is the same as $v_a(\phi)$ across the whole width of the die outlet. The flow rate via the die can be modified by using the constraint function g_2 [45].

So, when the mean velocity at the die exit v_a is the same as the required gap-wise mean velocity at the exit $\bar{v}_{\mathrm{p}}$, the needed overall flow rate *Q* which the die is operating is given by [45];

$$Q = 2h_{exit}\int_{l_{exit}} \bar{v}_p\, dx, \tag{3.3.6}$$

In Eq. 3.3.1, the input pressure P_{in} can change depending on the design to obtain certain *Q*. This formula gives a way of enforcing the uniformity of exit velocity with g_1 and the total flow rate with g_2 single-handedly. This allows for greater design flexibility than previous optimization methods [26]. The half-height *h(x, y)* in the die cavity can be chosen at will. So, constraints g_3k, where *K* = 1, 2... *Ns* are put in place to make sure that the gradient of *h(x, y)* stays within the specified estimate $\| \nabla h_p \|$ [45]. This is done to prevent extensional flows, which would otherwise make the assumptions of the flow model invalid.

In contrast to the constraints $g_1(\phi)$ and $g_2(\phi)$, which depend indirectly on the design variables through the governing equations, the objective function $f(\phi)$ and constraint ${g_3}^k(\phi)$ depend directly on the design variables [45]. Due to this concealed dependence, the design sensitivity analysis becomes more difficult.

Equation 3.3.4's objective function f (ϕ) and constraint $g_3{}^k$ (ϕ) are both defined explicitly on ϕ, making it easy to calculate design sensitivity [44]. Equation 3.3.9 allows one to compute the sensitivity analysis of the objective function $f(\phi)$ using the following:

$$\frac{Df(\phi)}{D\phi_i} = 1 \; for \; \phi_i = P_{in} \, , otherwise = 0, \tag{3.3.7}$$

Using a similar approach, the sensitivity for the constraint $g_3{}^k$ is as follows:

$$\frac{Dg_3^k(\phi)}{D(\phi_i)} = 0, \text{ for } \phi_i = P_{in} \tag{3.3.8}$$

Otherwise, equation 3.38 becomes

$$\frac{Dg_3^k(\phi)}{D(\phi_i)} = \frac{1}{\|\nabla h\|\|\nabla h_p\|}. \tag{3.3.9}$$

where the gradients of 1/2 height, *h*, are calculated at the K-th element only. These functions g_1 (ϕ) and g_2 (ϕ) in Eq. 3.3.1 are defined implicitly by the solution found by solving Eq. 46 with the Ansys Fluent Solver [46].

$$f(\phi) = G(P(\phi), \phi), \tag{3.3.10}$$

F is one of the two potential implicit constraints; it is defined by a function G, which is directly influenced by the design parameter and indirectly by ϕ through the nodal pressure vector *P* [46]. The adjoint variable approach can be employed to ascertain the sensitivity of *F* to variations in the design variable ϕ_i, provided that the surface is suitably smooth.

$$\frac{Df}{D\phi_i} = \frac{\partial G}{\partial \phi_i} - \boldsymbol{\lambda}.\frac{\boldsymbol{\partial R}}{\boldsymbol{\partial \phi_i}}, \tag{3.3.11}$$

where the adjoint variable vector ƛ is calculated from the system of linear equations

$$\left[\frac{\partial \boldsymbol{R}}{\partial P}\right]^T \boldsymbol{\lambda} = \left(\frac{\boldsymbol{\partial G}}{\boldsymbol{\partial P}}\right)^{\boldsymbol{T}}. \tag{3.3.12}$$

The ratio ∂G/∂P (sign partial derivatives cannot be bold) for the specified performance metric represents the adjoint load. The computational expense of the adjoint variable technique is diminished as it necessitates the analysis of only one linear adjoint problem, as specified by Equation 3.3.12, for each implicit objective and constraint function [4]. In addition, it uses the

transpose of the tangent matrix $\left[\frac{\partial \boldsymbol{R}}{\partial P}\right]^T$ from Eq. 3.3.11 to drastically minimize the computational work required by the N-R iteration for the pressure solution. For every $\partial G/\partial \phi_i$, 0, ϕ_i, i = 1... N, the constraints g_1, and g_2 in Eq. 3.3.2 and 3.3.3, respectively are independent of the design variables under consideration. However, these restrictions rely on the pressure solution being passed through.

3.1.4 Flowchart for Adjoint

To run the Adjoint solver, the CAD file is first generated using SolidWorks. The ANSYS Fluent is then used to generate a mesh and run the initial solution using the boundary conditions and material law described initially. This solution from this first simulation serves as input to the Adjoint solver for further optimization. Then, the observable and bounds, regions, and target change are defined. The design change is then calculated, and the first iteration for optimization is done; after this, the Adjoint solver is allowed to run for 20 iterations using the scheme program developed from the SCHEME programming language. Iterations are repeated until there is no further improvement in the design. The flowchart for the Adjoint optimization is shown in Figure 3.2 below.

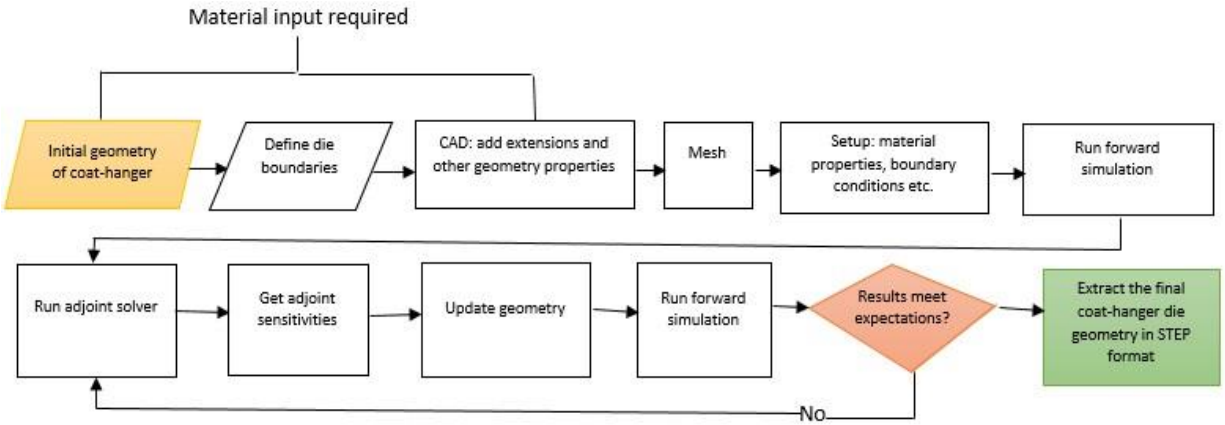

Figure 3.2: Adjoint Optimization Technique Flowchart

Chapter 4 – Design of the Die Body Using Fluid-Structure Interaction

4.0 General

This section shows the results from the FSI study of the die body. First, a mesh independence study is carried out for both fluid and solid bodies to ascertain the best mesh size for the simulation. Subsequently, a 2-way FSI is used to determine the best die body that will eliminate die deflection at the exit of the die.

4.1 Results and Discussion

4.1.1 Mesh Independency Study

Figure 4.1 shows the mesh independence study for the fluid and solid domain of the coat-hanger die respectively. Initially, mesh elements of 20496 were used to initiate the independence study for the fluid domain. It was observed that mesh elements of 500,000 up to 1,000,000 had almost the same maximum outlet velocity value of $0.42ms^{-1}$. Also, 13,551 mesh elements were used to initiate the independency study for the solid domain and it was observed that mesh elements of 200,000 and above had almost the same maximum deflection of 0.00266mm. Hence, a mesh size of 1 mm, which gives mesh elements of over 700,000, was used for the fluid body, and a mesh size of 3 mm was used for the solid domain, as shown in Figure 4.2.

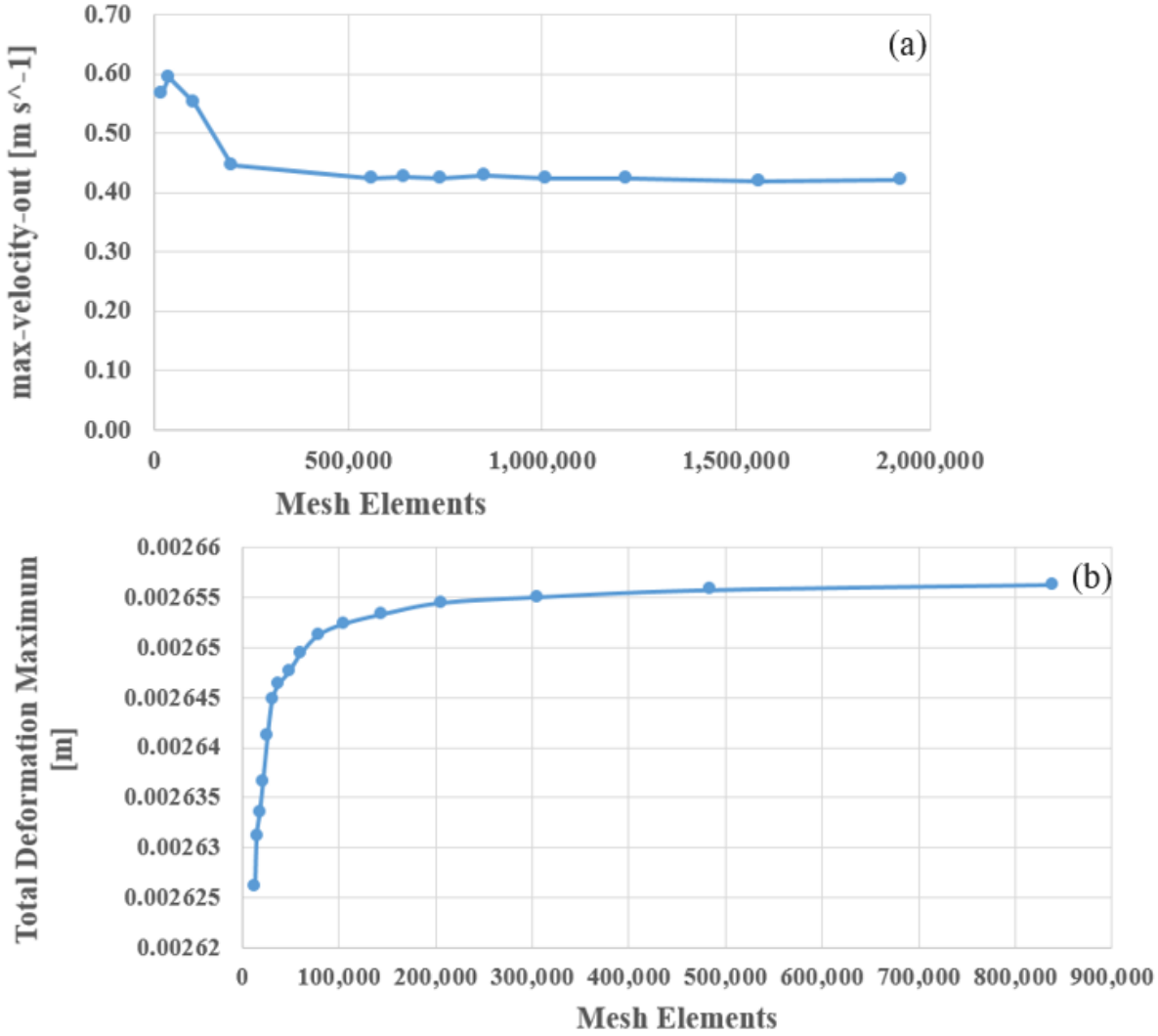

Figure 4.1: Mesh Independency Study of (a) Fluid body and (b) Solid body

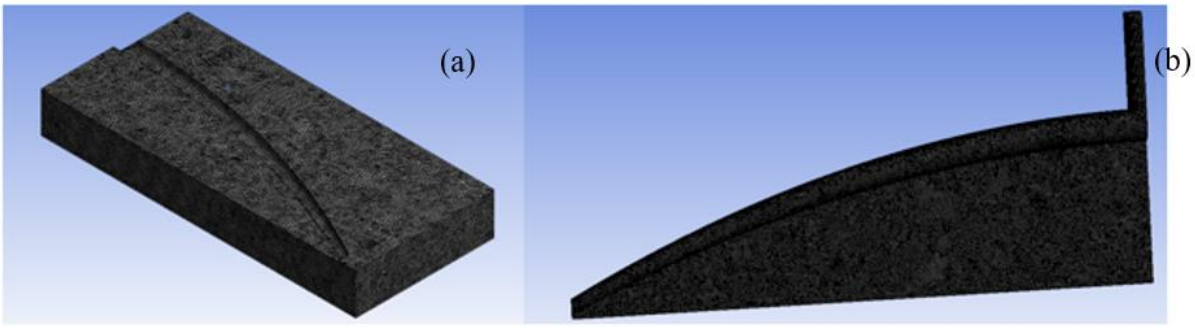

Figure 4.2: Meshing for die body (a) and fluid body (b)

4.1.2 Pressure Distribution Using Different Material Law

Figure 4.3 shows the distribution of pressure along the die for the various rheological models. It was observed that the power law model generated higher maximum pressure in the die, which was 7.6 MPa, while the cross rheological model generated a maximum pressure of 7.02 MPa. The maximum pressure generated in the die using the Carreau rheological model (4.18 MPa) was way smaller than the pressure generated by the two other models.

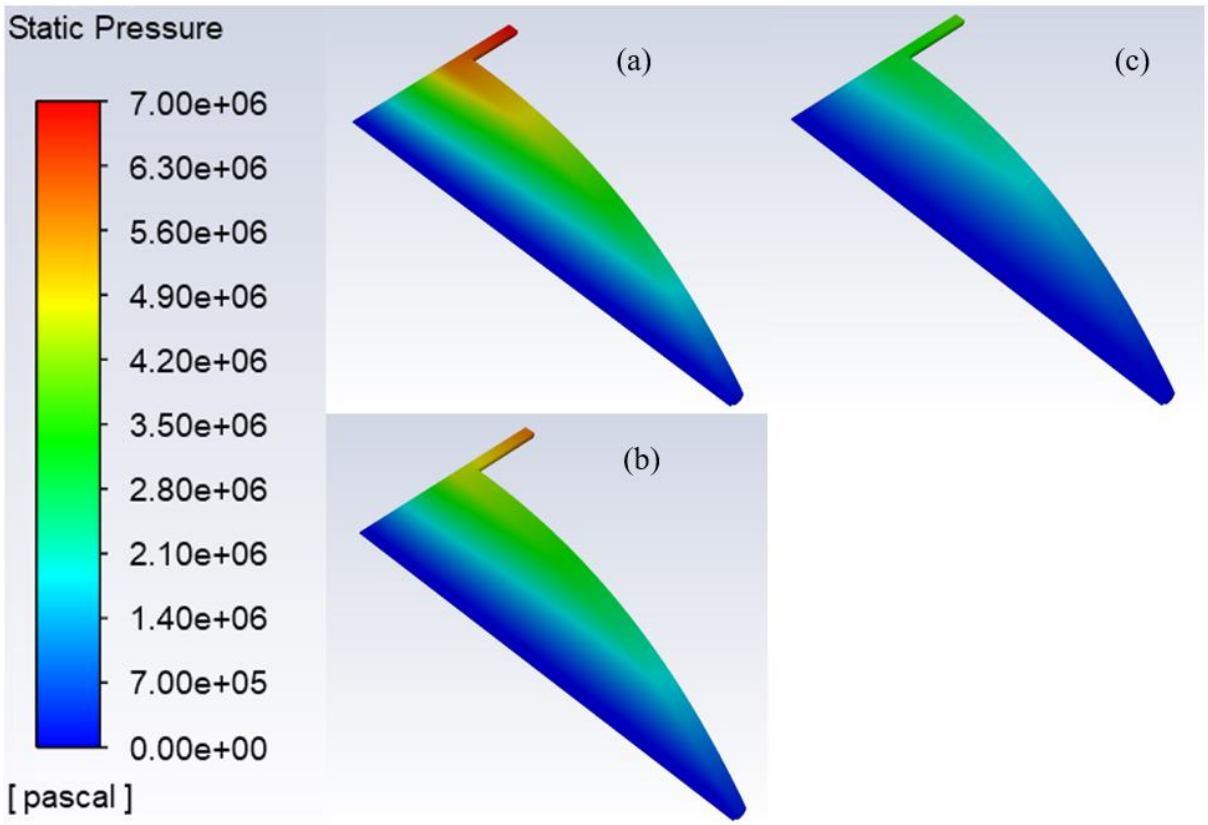

Figure 4.3: Pressure Distribution: (a) Power-law model (b) Cross model (c) Carreau-Yasuda model.

4.1.3 Deflection at the Exit for Different Material Laws

The die body deflection was maximum at the die outlet, as shown in Figure 4.4. It can be seen that the average deflection when using power law is 0.0093 mm; when the Cross model is used, it is 0.0075 mm, and it is 0.0052 mm when the Carreau model is used. The variations in the deflection for the various models result from pressure differences. Appendix A.1 shows the contour plot of the deflection for the different material laws. The maximum deflection in all cases occurs at the entrance of the manifold of the die due to factors like geometry, variations in material property, load distributions, support and stress concentrations. The center of the die

is more susceptible to higher deflection due to its relative position to the variations in these factors.

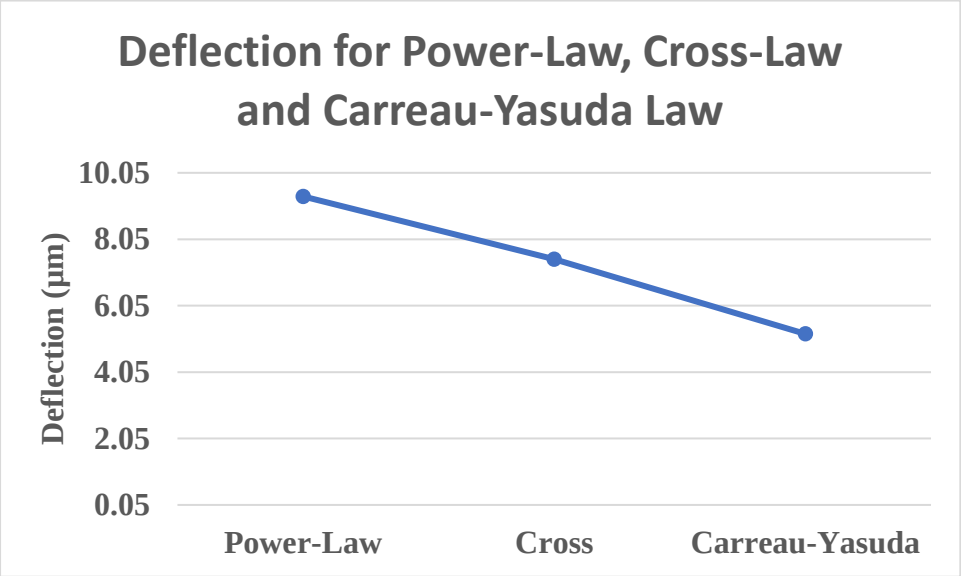

Figure 4.4: Total die exit deflection using Power-law model, Cross model and Carreau-Yasuda model.

4.1.4 Equivalent Stress and Equivalent Elastic Strain for Different Material Laws

The equivalent stress is a scalar quantity, which is a derivative of shear strain energy per unit volume measured at various points in a material under the influence of stress, and it helps to show the likelihood of failure of the material. The material fails when the equivalent stress exceeds the ultimate tensile strength (UTS). The equivalent stress in the die, as shown in Figure 4.5 and appendix A.2 when using power law, was 153.4MPa, 120.62MPa when using the Cross model and 85.44MPa when using the Carreau model. The ultimate tensile strength of tool steel which, adopted in the die body simulation is 2380MPa. Hence, for each of the model, the equivalent stress was far less than the ultimate tensile strength.

The equivalent elastic strain, as shown in Figure 4.5 and appendix A.2 represents the total strain energy stored in the material during deflection. The maximum equivalent elastic strain is higher using the power law model than the other models. Its value is 0.00073 for the power law, 0.00058 for the Cross law and 0.00041 for the Carreau law.

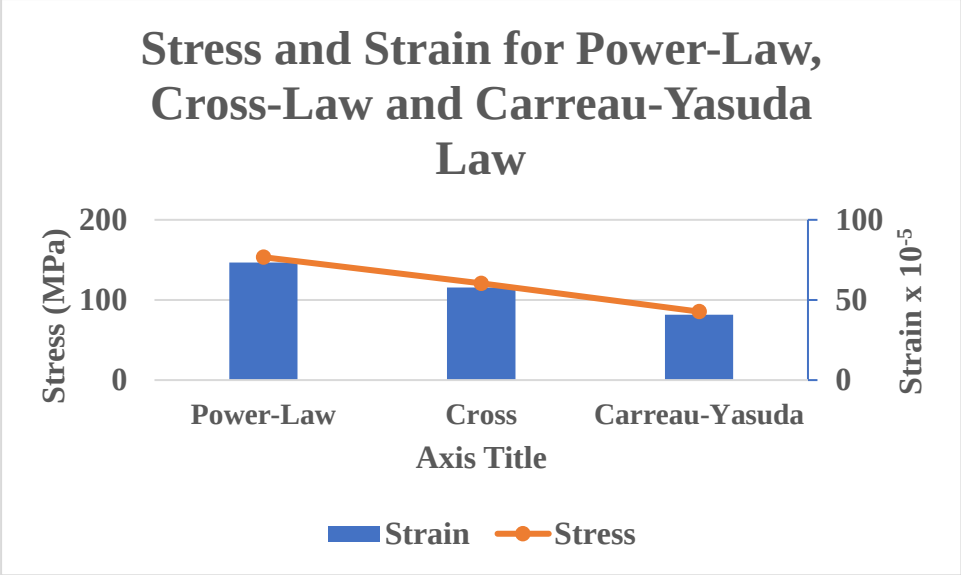

Figure 4.5: Equivalent Stress and Equivalent elastic strain using the Power-law model, Cross model, and Carreau-Yasuda model.

4.1.5 Deflection at the Exit Using Different Number of Bolts as Supports

Since we have been able to establish that the power law generates higher pressure within the die, which results in higher deflection, strain, and stresses along the walls of the die body, it becomes paramount to determine by what extent the deflection, strain and stresses in the die is reduced when the number of supports is increased. In industries, about eight holes are used as support in the die, but manufacturing these eight holes usually poses many challenges. Manufacturing a die with eight holes on either side takes much effort, and over a long period, the steel becomes weak due to higher stress concentrations around these holes on the die body. Hence, there is a need to reduce the support needed to enhance the ease of production of the dies and longevity. It can be observed that the maximum equivalent elastic strain while using any of the models occurred at the first bolt support (represented by the first hole) for the die. Along the fluid channel, elastic strain occurs almost up to the center.

From Figure 4.6 and appendix A.4, it can be observed that the changes in deflection values when the number of holes is increased are negligible between 0 and 4 holes. Average deflection is 0.00934mm, 0.00926mm, 0.00926mm, and 0.00924mm for 0, 2, 3, and 4 bolt support respectively.

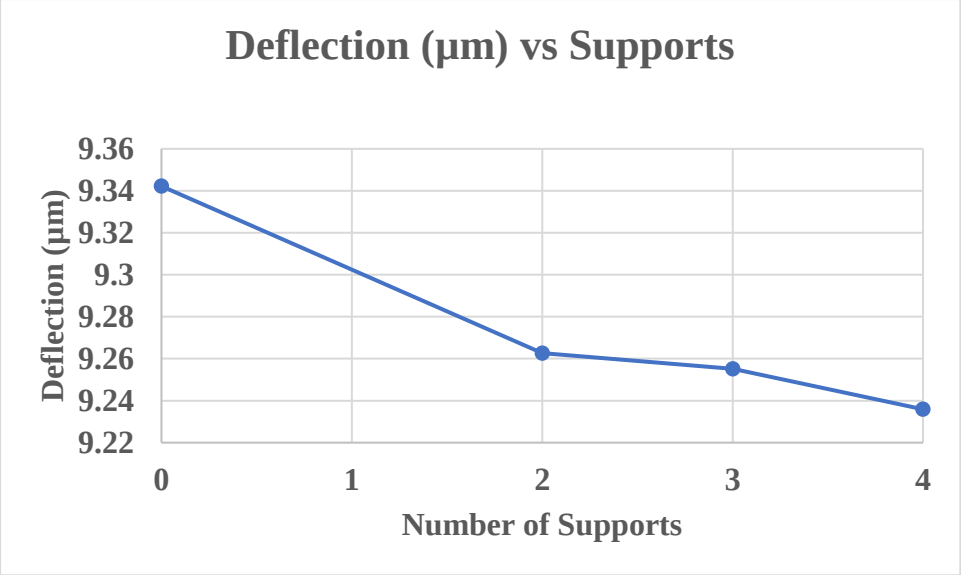

Figure 4.6: Deflection of the die exit using 0 bolts, 3 bolts, and 4 bolts.

4.1.6 Equivalent Stress and Equivalent Elastic Strain for Different Support

As shown in Appendix A.6, the equivalent stress is maximum at the edge of the manifold inlet and spreads mainly around the manifold section of the die body. As shown in Figure 4.7, the decrease in the equivalent stress was insignificant. In all four cases, the equivalent stress was at 153MPa.

Also, the maximum equivalent elastic strain in the die body is 0.000734 for 0-bolt support, 0.000728 for 2-bolt support, 0.000719 for 3-bolt support, and 0.000736 for 4-bolt support. This is shown in Figure 4.7 and Appendix A.5.

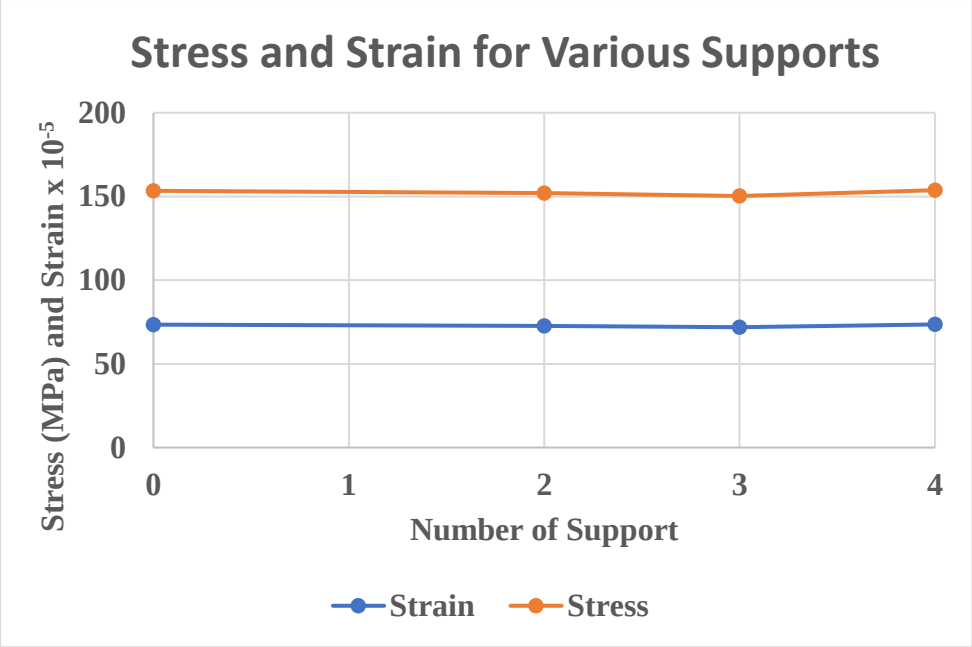

Figure 4.7: Equivalent stress and elastic strain using 0, 2, 3, 4 and 5 support holes.

As shown in figure 4.8, the shear stress around the regions where there are supports, is zero. Although, there is shear stress around the end of the first support hole, this value is very small and negligible.

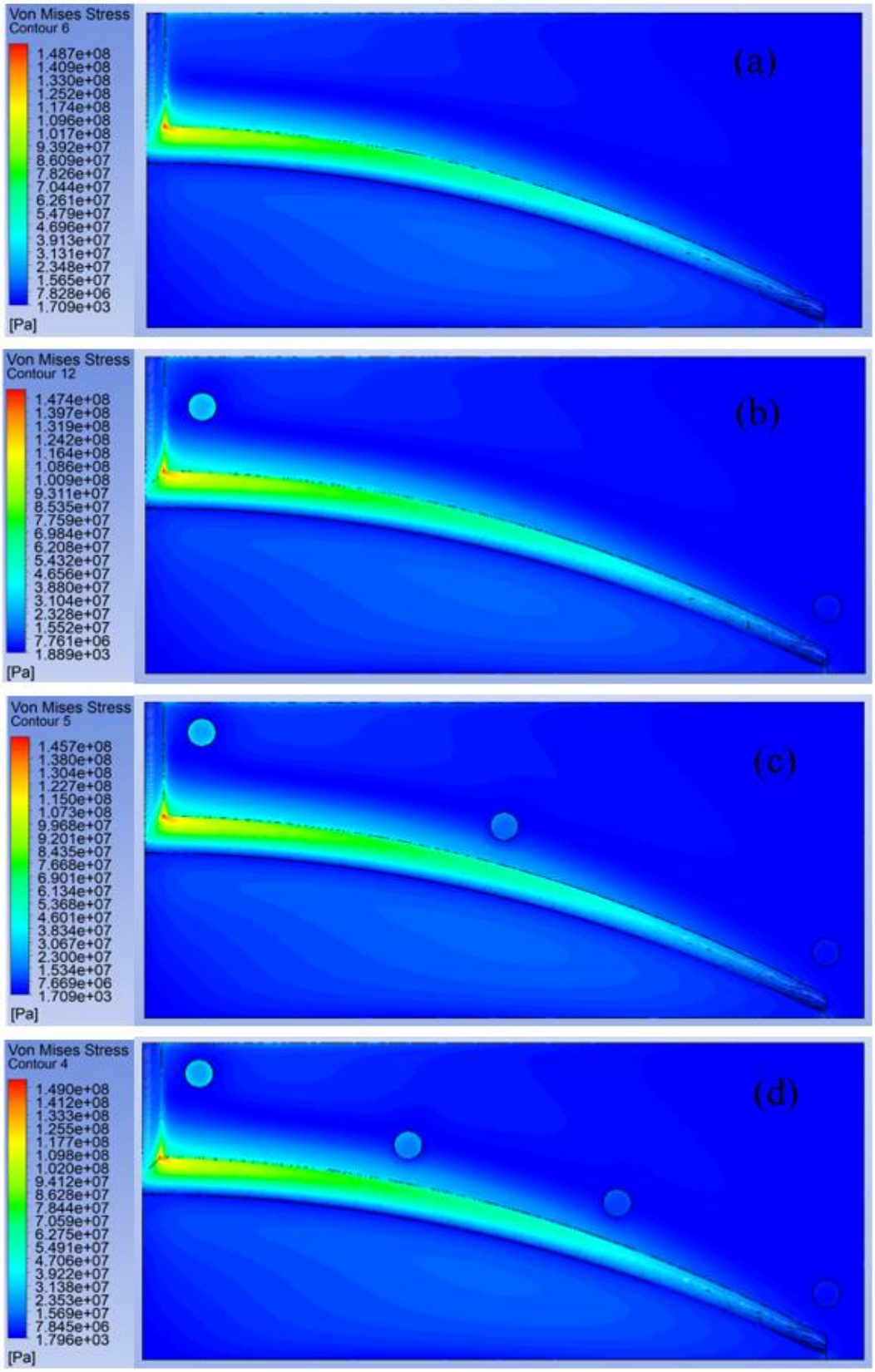

Figure 4.8 Equivalent Stress at various Planes for (a) 0 (b) 2 (c) 3 (d) 4 and (e) 5 supports.

4.1.7 Die Deflection at Exit for Different Die Body Thickness

Since the deflection at the exit is still very high, up to 4.9% when the thickness of 30mm and 4-support bolts are used, there is a need to reduce this deflection further to meet the high performance of the die. It can be observed from Figures 4.8 and 4.9 that increasing the die body thickness from 30mm to 100mm reduces the average deflection from 0.0092mm to 0.0034mm, which is a 63.04% improvement, which represents 1.03% die exit deflection.

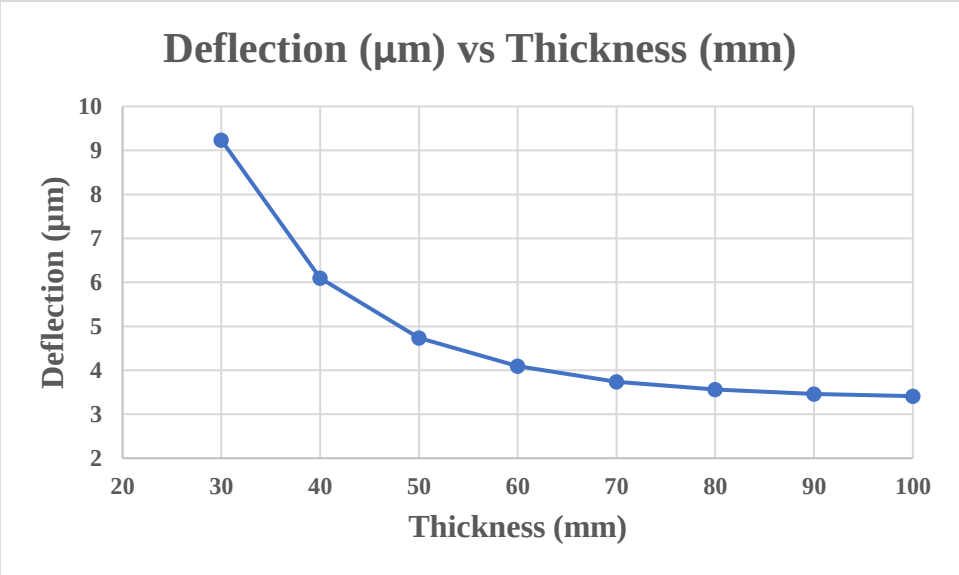

Figure 4.8*: Deflection for Various Die Body Thickness (mm)*

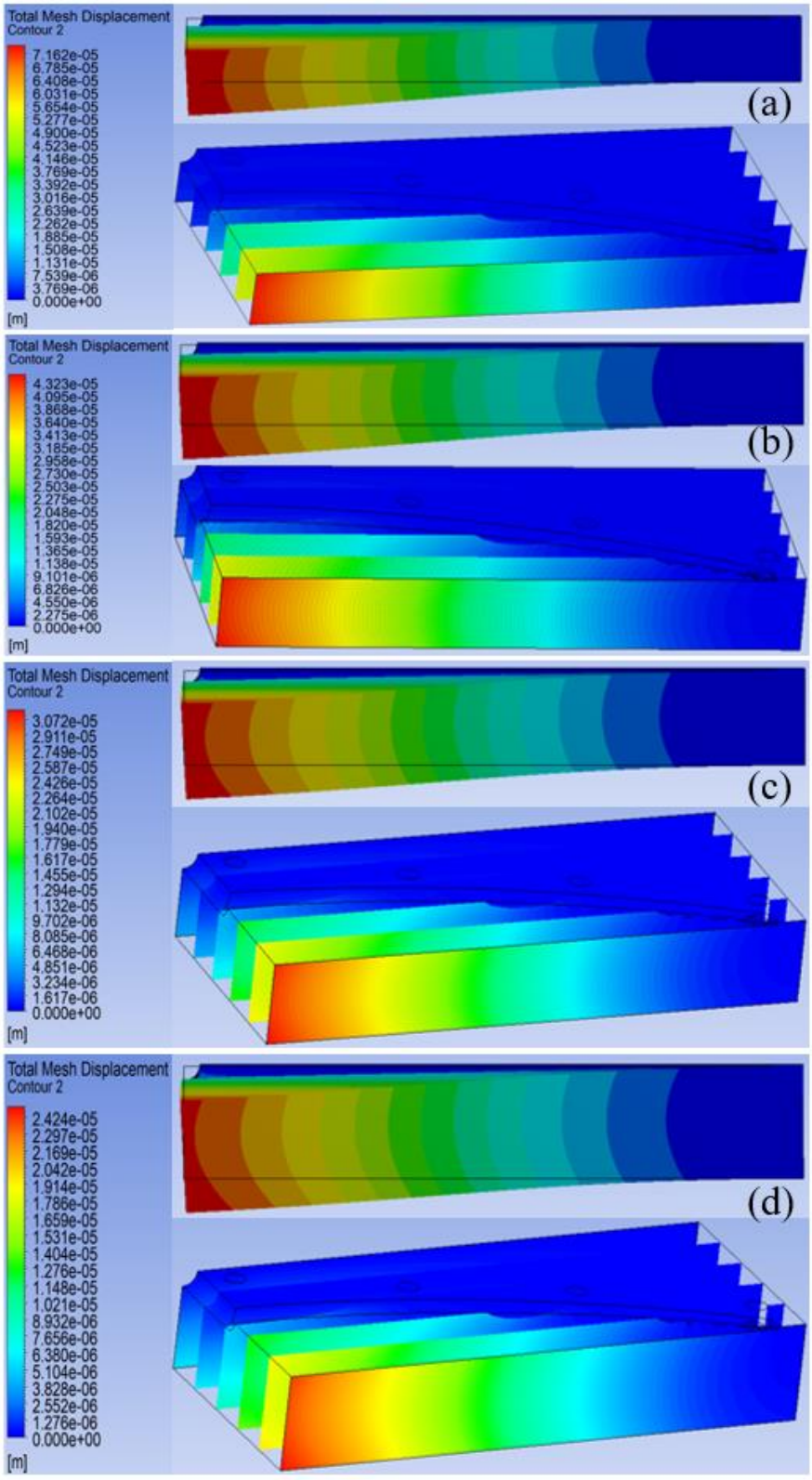
Total Mesh Displacement
Contour 2
7.162e-05
6.785e-05
6.408e-05
6.031e-05
5.654e-05
5.277e-05
4.900e-05
4.523e-05
4.146e-05
3.769e-05
3.392e-05
3.016e-05
2.639e-05
2.262e-05
1.885e-05
1.508e-05
1.131e-05
7.539e-06
3.769e-06
0.000e+00
[m]
(a)
Total Mesh Displacement
Contour 2
4.323e-05
4.095e-05
3.868e-05
3.640e-05
3.413e-05
3.185e-05
2.958e-05
2.730e-05
2.503e-05
2.275e-05
2.048e-05
1.820e-05
1.593e-05
1.365e-05
1.138e-05
9.101e-06
6.826e-06
4.550e-06
2.275e-06
0.000e+00
[m]
(b)
Total Mesh Displacement
Contour 2
3.072e-05
2.911e-05
2.749e-05
2.587e-05
2.426e-05
2.264e-05
2.102e-05
1.940e-05
1.779e-05
1.617e-05
1.455e-05
1.294e-05
1.132e-05
9.702e-06
8.085e-06
6.468e-06
4.851e-06
3.234e-06
1.617e-06
0.000e+00
[m]
(c)
Total Mesh Displacement
Contour 2
2.424e-05
2.297e-05
2.169e-05
2.042e-05
1.914e-05
1.786e-05
1.659e-05
1.531e-05
1.404e-05
1.276e-05
1.148e-05
1.021e-05
8.932e-06
7.656e-06
6.380e-06
5.104e-06
3.828e-06
2.552e-06
1.276e-06
0.000e+00
[m]
(d)

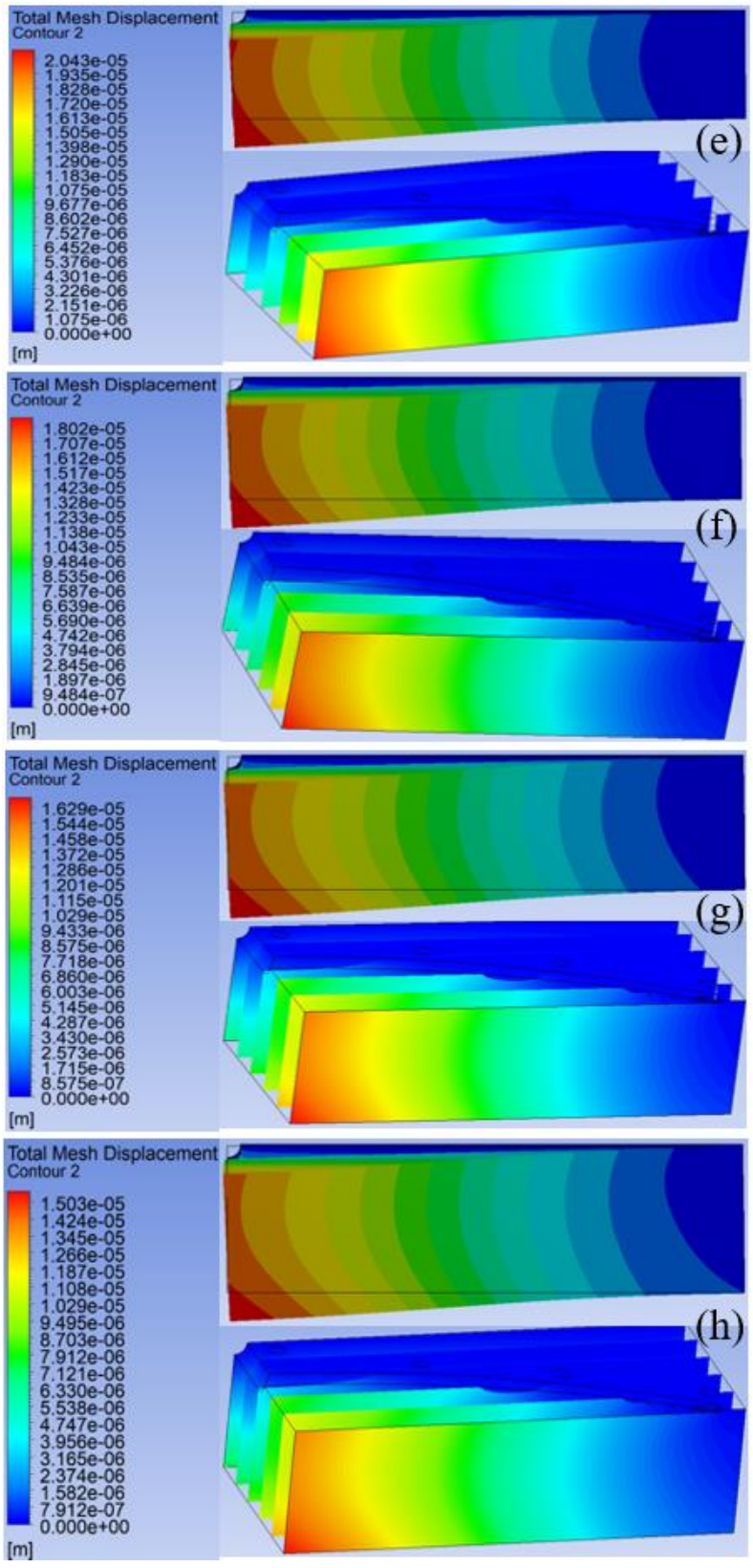

Figure 4.9: Deflection at Die Exit for (a) 30mm (b) 40mm (c) 50mm (d) 60mm (e) 70mm (f) 80mm (g) 90mm (h) 100mm.

4.1.8 Equivalent Stress and Equivalent Elastic Strain for Different Thickness

Figure 4.10, Appendices A.7 and A.8 shows the equivalent stress and strain of various die body thicknesses. It can be observed that higher stresses and strains occur in the die when the die body's thickness is small compared to when the thickness is high. The stresses in the die thickness of 30mm are 153.7MPa, which is reduced to 84.1MPa when the thickness is increased to 100mm. Also, the equivalent strain is reduced from 0.000734 to 0.000402 as the thickness increases from 30mm to 100mm.

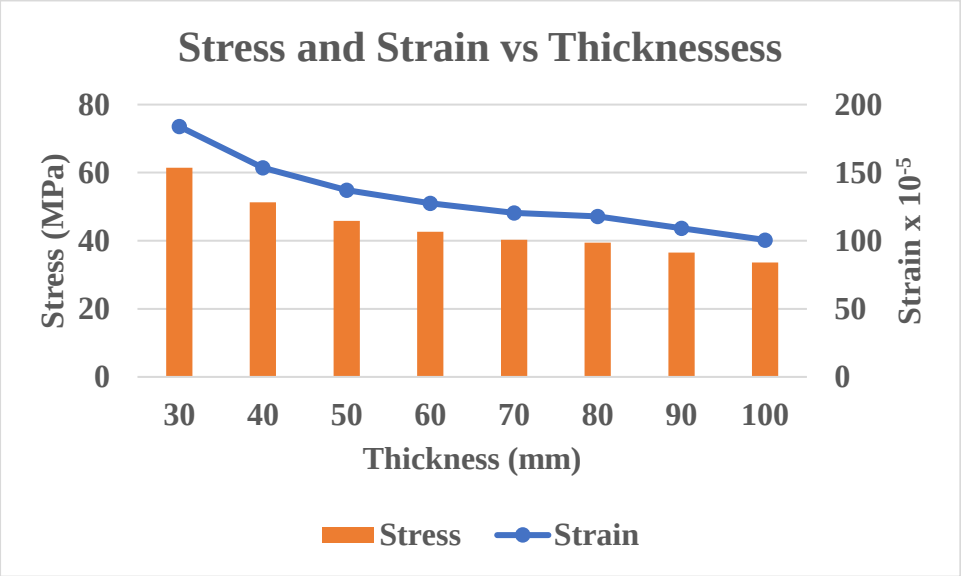

Figure 4.10: Stress and Strain for Various Die Body Thickness

4.2. Concluding Remarks

As melt flows, it exerts internal Pressure on the die wall, which eventually causes die deflection at the exit. This deflection at the exit reduces the uniform distribution of velocity and increases the Pressure loss, which leads to poor die performance. Hence, there is a need to reduce the die deflection at the exit, especially at the center of the die, to enhance the die performance. The standard die used in the industry has eight support bolts on each side; it is observed that producing a die with eight support bolts can become very difficult, and due to stress concentration being higher in these regions, the steel material becomes weaker over time; this is why we have reduced the number of supports from 8 to 4.

It can be observed that reducing the die support to 4 and increasing the thickness to 100mm reduces the maximum deflection from 0.0739mm (deflection at 30mm) to 0.0155mm, a 63.04% improvement, representing a 1.03% die exit deflection. Also, the maximum stress concentration is reduced from 153.4MPa to 84.1MPa, while the maximum strain concentration is also reduced from 0.000734 to 0.000402 as the thickness increases from 30mm to 100mm.

Chapter 5 – CFD Analysis of Existing Die and Adjoint Optimization

5.0 General

This chapter analyzes the existing die design based on two commonly used material laws (Power law and Carreau-Yasuda law) and optimizes the existing die using the adjoint method. First, the pressure drop between the inlet and outlet of the fluid body of the die is used as an observable. This reduces the pressure drop in the die and reduces power consumption. Afterward, the mass flux variance is further used as an observable to enhance the uniformity of the velocity at the exit.

5.1 Results and Discussion

5.1.1 Comparison of Vector of Velocity Distribution at the Exit for Different Material Laws

Figure 5.1 shows the vector of velocity contour for Power law and Carreau-Yasuda law. The velocity distribution uniformity is higher in the Power law than in the Carreau-Yasuda law. Since most of the polymeric melts are non-Newtonian, optimizing the fluid body of the die using a non-Newtonian material law is necessary. Hence, the Carreau-Yasuda law was adopted to optimize the fluid body further.

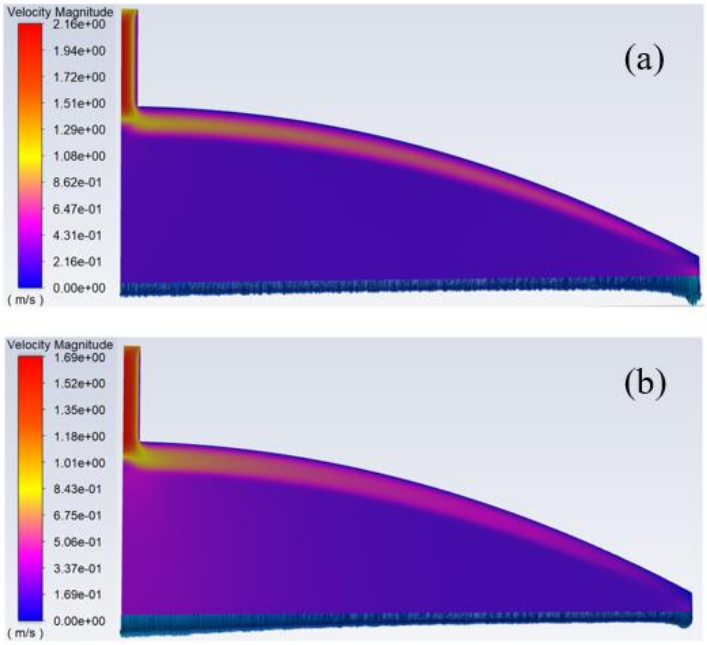

Figure 3: Contour of Velocity Vector for (a) Power-law and (b) Carreau-Yasuda law.

5.1.2 Adjoint Optimization Using Pressure drop and Mass-Flux-Variance as Observables

For us to fully optimize the fluid body of the die for optimal performance of uniform velocity distribution and reduced pressure drop, we need to combine these two objectives as the observables for Adjoint optimization. First, the pressure drop was used as an observable to reduce pressure drop, while subsequently, the mass-flux-variance was used to increase the uniformity of the velocity at the exit. As shown in Figure 5.2, iterations were performed for the pressure drop, and this reduced the pressure from 3990651.3 Pa to 3350517.8 Pa (16.04% reduction). In comparison, 24 iterations were performed using the mass-flux-variance, and this reduced the mass-flux-variance from 0.025834378 $kg/m^{-2}s^{-1}$ to 0.011228295 $kg/m^{-2}s^{-1}$ (56.54% reduction).

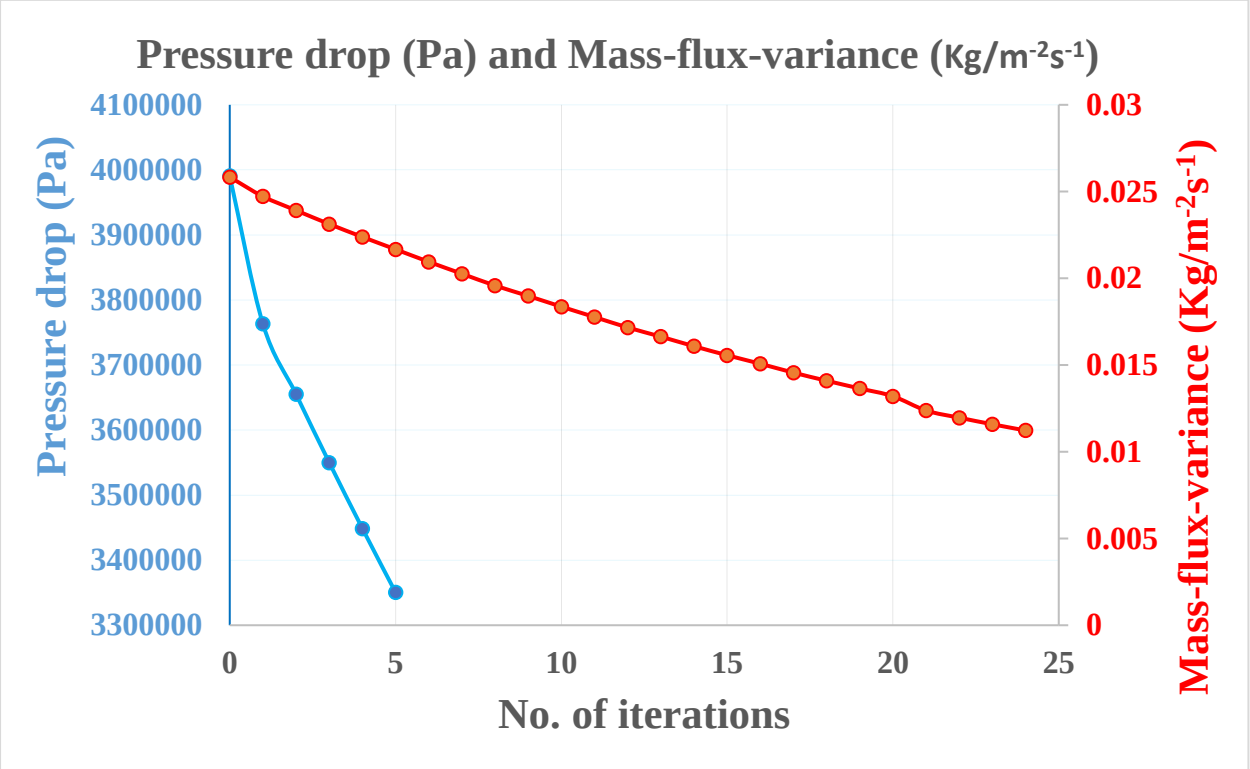

Figure 4: Plot of Adjoint Optimization for Observable: Pressure drop and Observable: Mass-flux-variance for Various Iterations

5.1.3 Pressure Distribution for Various Designs

Figures 5.3 and 5.4 show the pressure drop distribution comparison for the initial die, observable: pressure drop and observable: Mass-flux-variance designs were taken from different distances from the center on the die, as shown in Appendix B.3. The pressure drop obtained by using the pressure drop as observable is higher than the initial and observable mass-flux-variance. Hence, the observable: pressure drop and mass-flux-variance perform better in reduced pressure drop than the initial die.

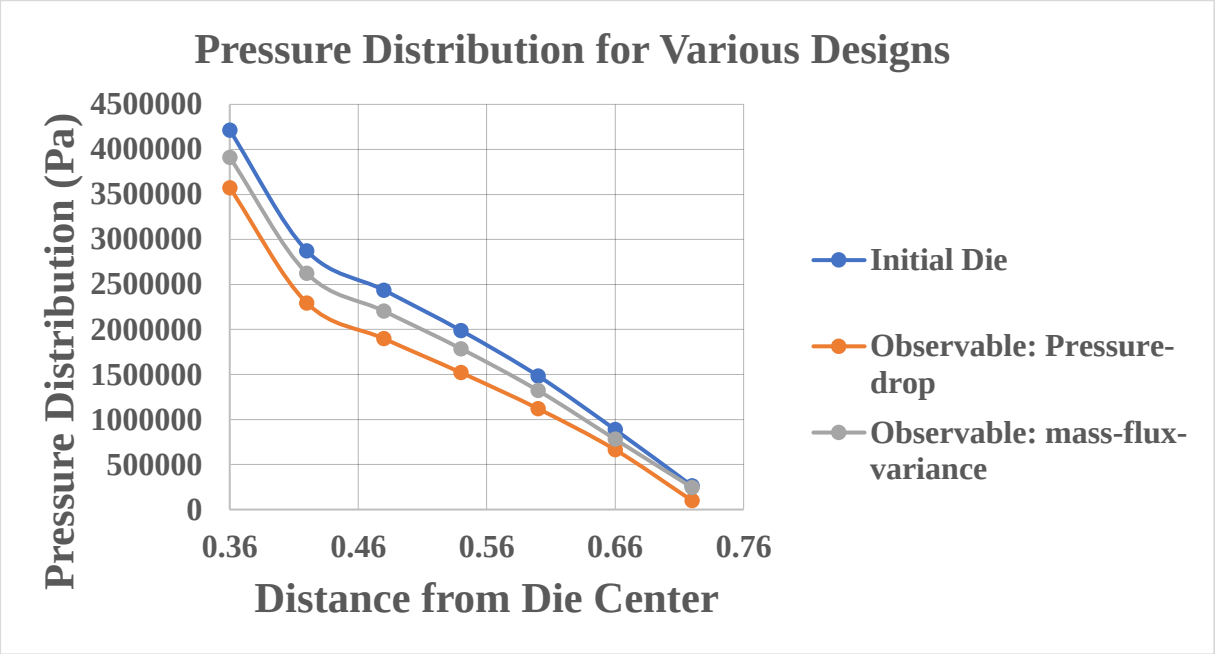

Figure 5: Pressure drop Distribution at Various Distance from Die Center for Different Die Designs

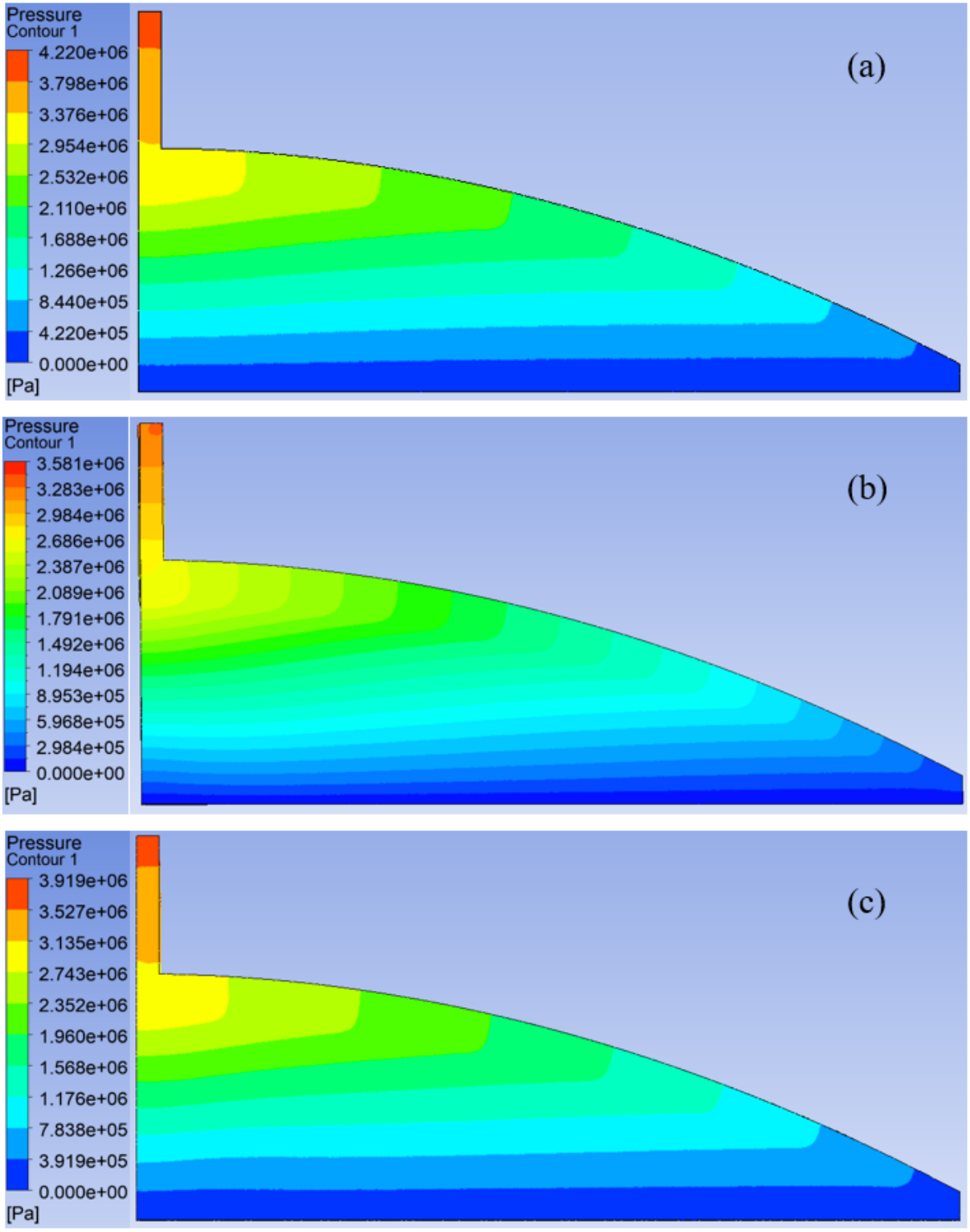

Figure 6: Pressure Contour for (a) Initial (b) Observable: Pressure drop and (c) Observable: mass-flux-variance Die Designs

5.1.4 Velocity Distribution for Various Designs

Even though the observable pressure drop performs better in terms of reduced pressure drop, the velocity distribution non-uniformity at the die exit is higher as compared to the initial die and observable: mass-flux-variance designs as shown in Figures 5.5, 5.6, and Appendix B.1. This is why only five iterations of the pressure drop were performed while using the observable: pressure drop because as the pressure drop decreases, standard deviation increases and the uniformity of the velocity decreases, as shown in the table 5.1. Hence, when the mass-flux-variance is used as an observable, the die design produces a die with enhanced uniformity of up to 0.86 out of 1.

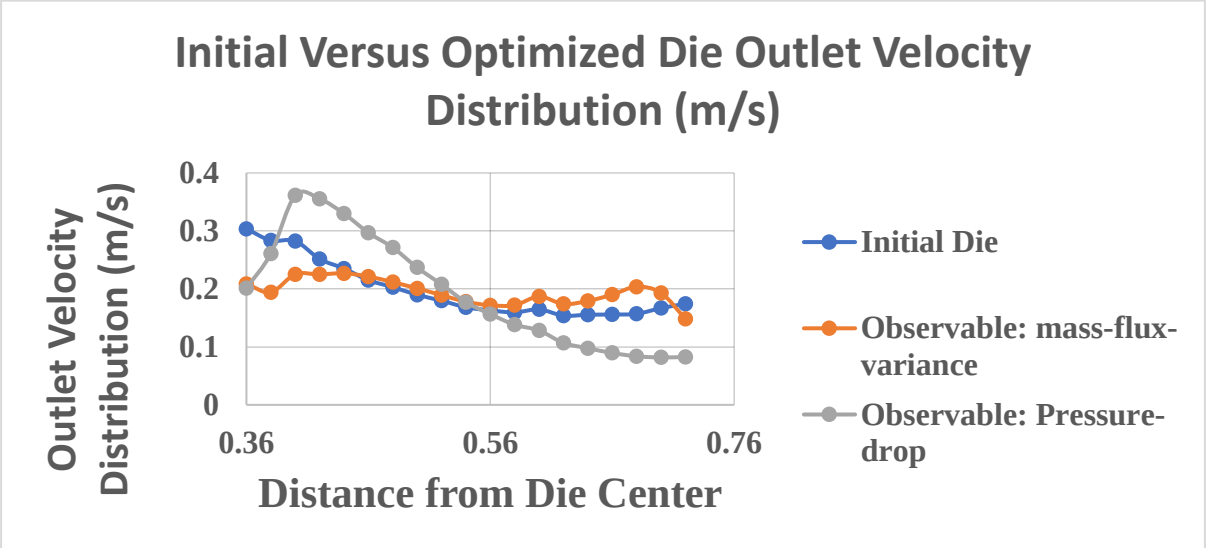

Figure 7: Die Outlet Velocity at Different Locations from Die Center for Various Design

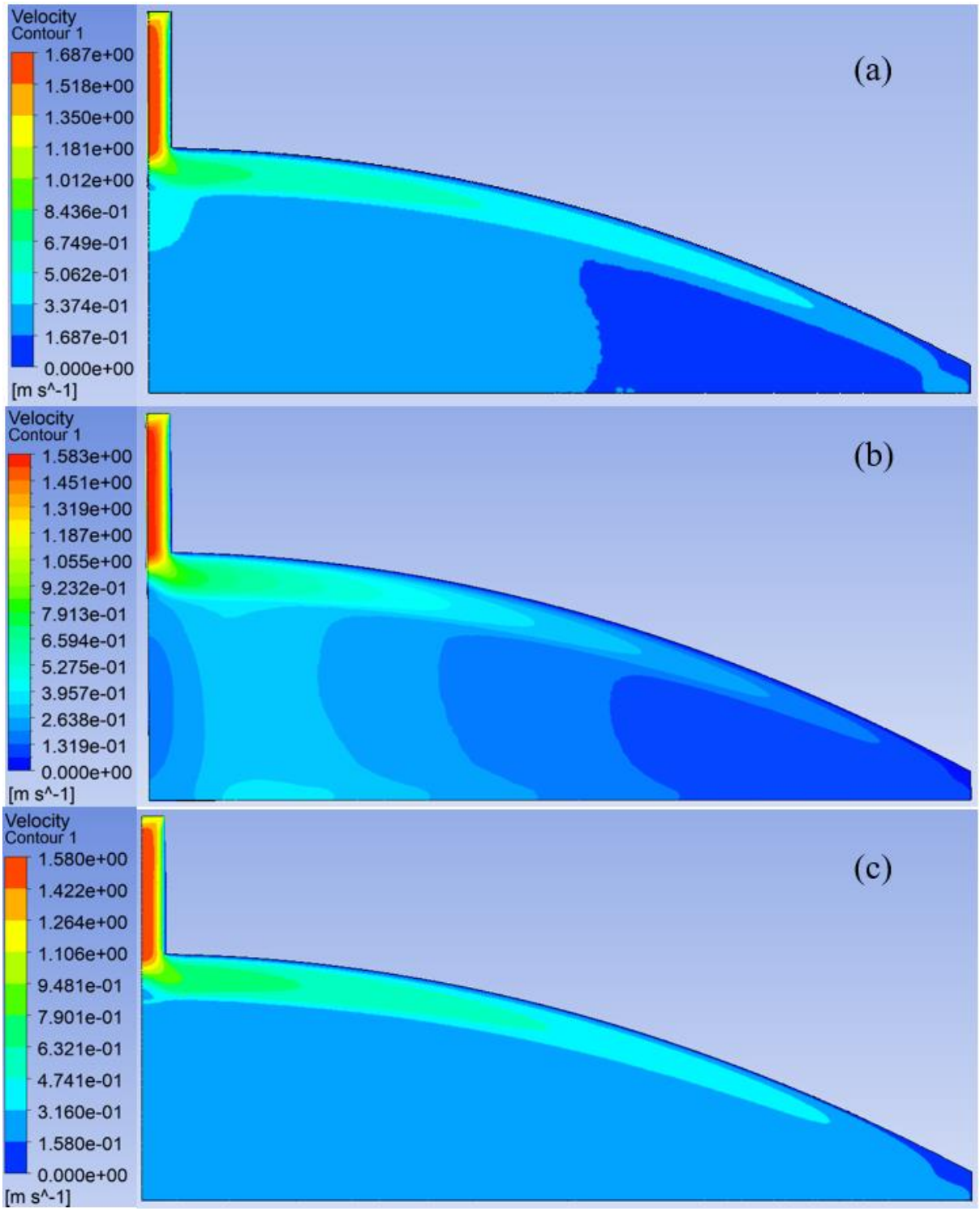

Figure 5.6: Velocity Contour for (a) Initial (b) Observable: pressure drop and (c) Observable: mass-flux-variance Die Designs

Table 5.1: Surface Integral Report for Various Die Design

Parameter	**Initial Die**	**Observable: Pressure drop**	**Observable: Mass flux**
Standard Deviation	0.070	0.092	0.062
Uniformity Index	0.844	0.745	0.861
Mass Flux Variance	0.0124	0.0258	0.011

Also, Figure 5.7 shows there was no stagnation zones for the different die designs.

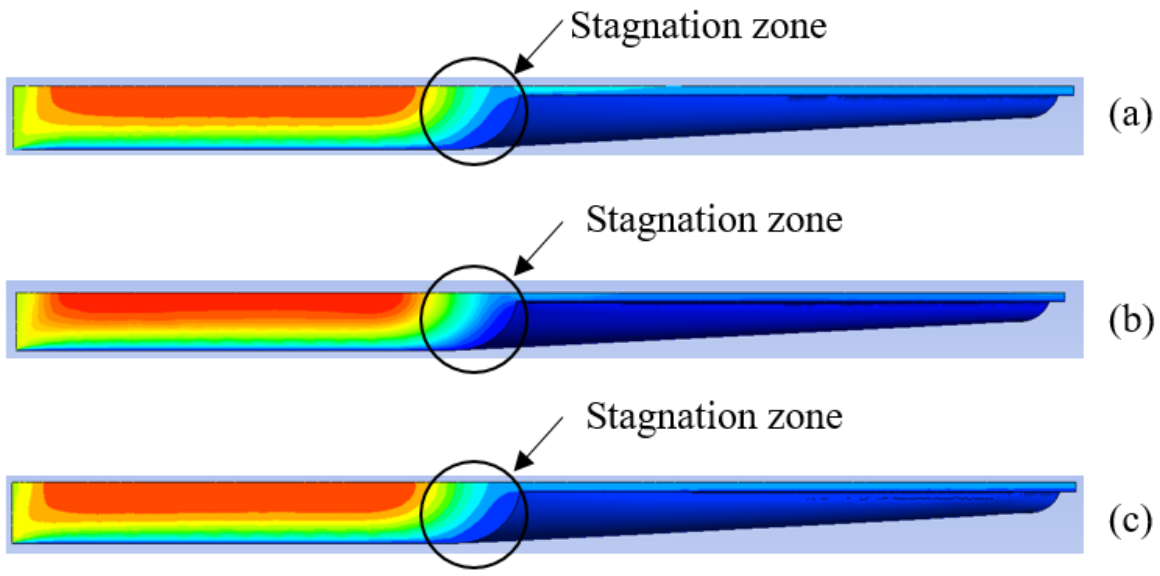

Figure 8: Stagnation Zone for (a) Initial (b) Observable: pressure drop and (c) Observable: mass-flux-variance Die Design

5.1.5 Wall Shear Stress Distribution for Various Designs

The distribution of the shear stresses at the Wall of the die at different planes from the die center is presented in Figures 5.8 and 5.9. The maximum and minimum shear stresses at the wall of the die, as shown in Figure 5.8, are 65KPa and 16.4KPa, 64KPa and 12.4KPa and 64.2KPa and 30.6KPa for the initial die, observable: pressure drop and observable: Mass-flux-variance designs, respectively. The shear stress distribution is more uniform in observable mass-flux-variance die designs than in the initial die and observable pressure drop die designs.

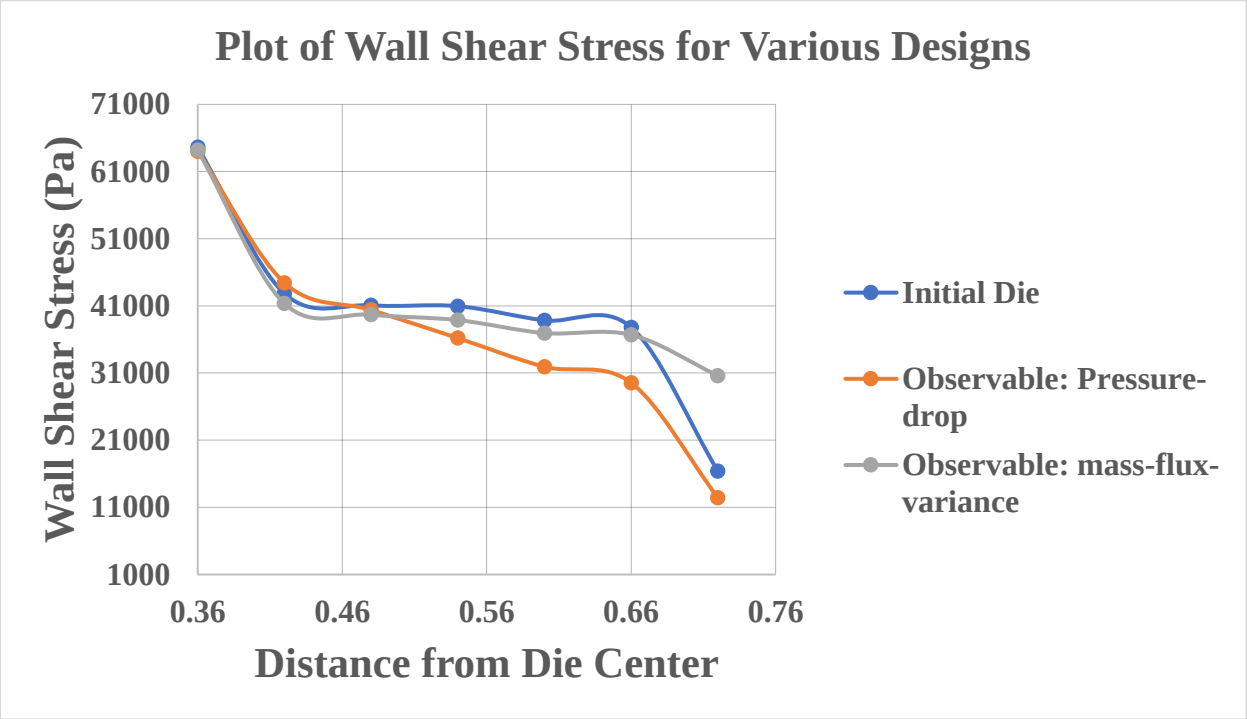

Figure 9: Wall Shear Stress for Various Die Designs

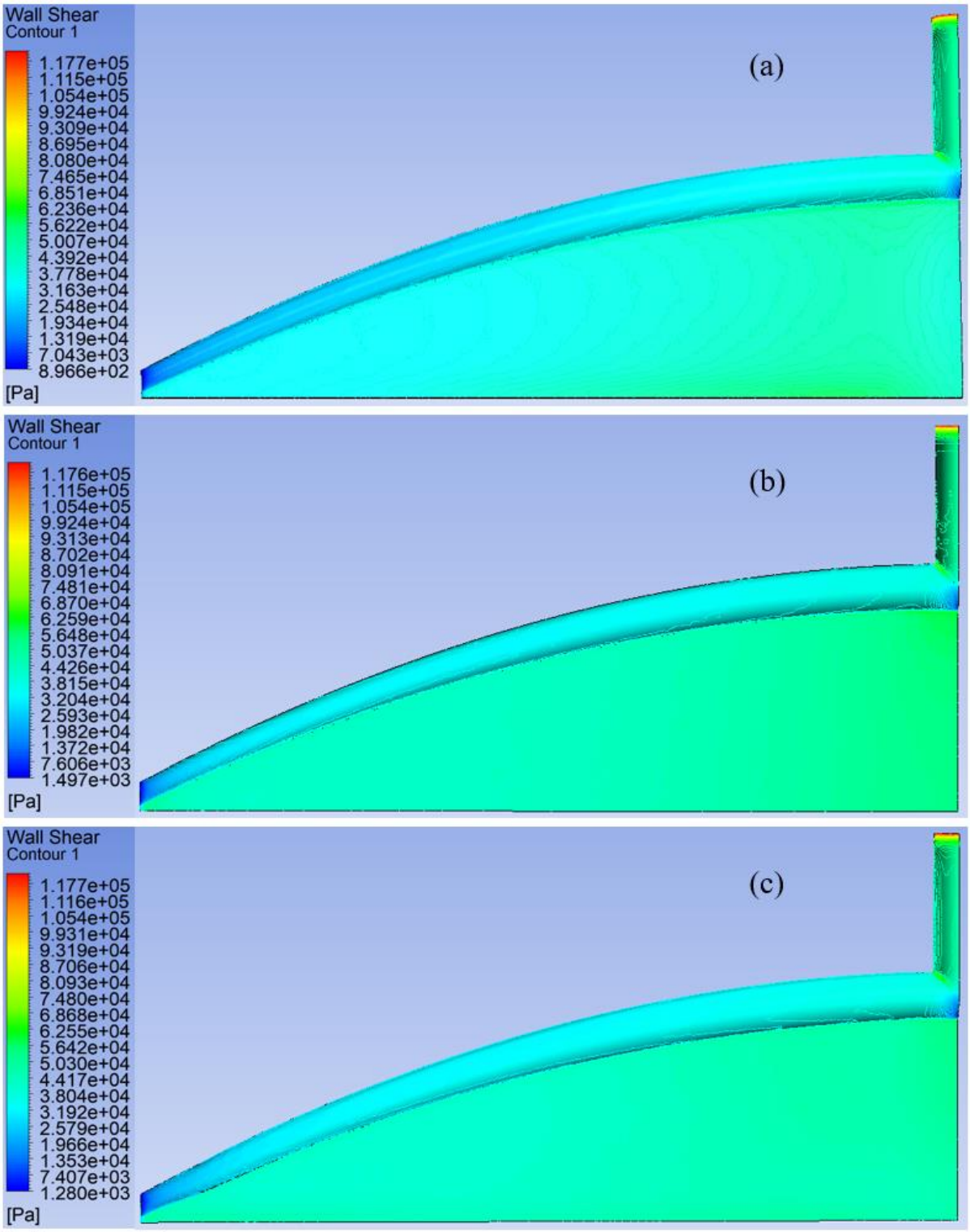

Figure 10: Wall Shear Stress for (a) Initial (b) Observable: pressure drop and (c) Observable: mass-flux-variance Die Design

5.1.6 Comparison of the Uniformity of the Exit Velocity between Initial and Optimized Die Designs

The velocity distribution at the die exit for the initial and optimized die design is shown in Figure 5.10 and Appendix B.2. It can be observed that the velocity distribution at the exit is more uniform in the optimized die than in the initial die design.

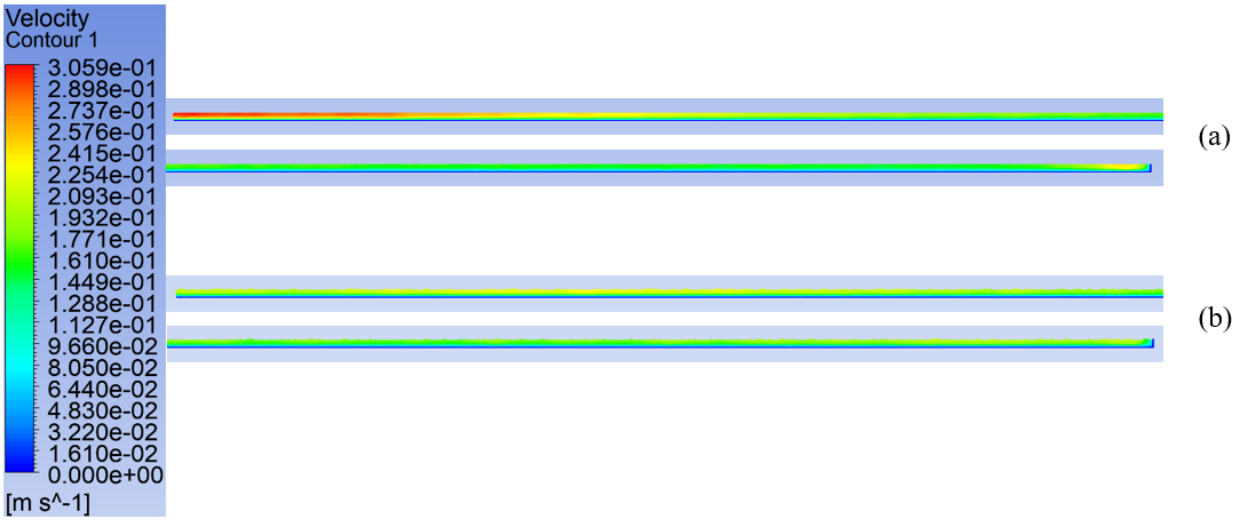

Figure 5.10: Velocity Distribution at Die Outlet for (a) Initial and (b) Optimized Die

5.1.7 Fluid Body Displacement

While using the adjoint solver, some parts of the fluid body of the die increase, decrease, or remain unchanged. Figure 5.11 shows the displacement of the fluid body for both observable: pressure drop and mass-flux-variance. Parts where the volume increases are indicated by a positive value, parts where the volume decreases by a negative value, and parts where there was no change remain blue. The volume increase was maximum around the manifold and outlet regions of the die while using the pressure drop as observable, and there was only a tiny decrease around the die walls. However, while using the mass-flux-variance as observable, the maximum increment was around the walls of the die and the manifold, and there was a reduction in the die volume.

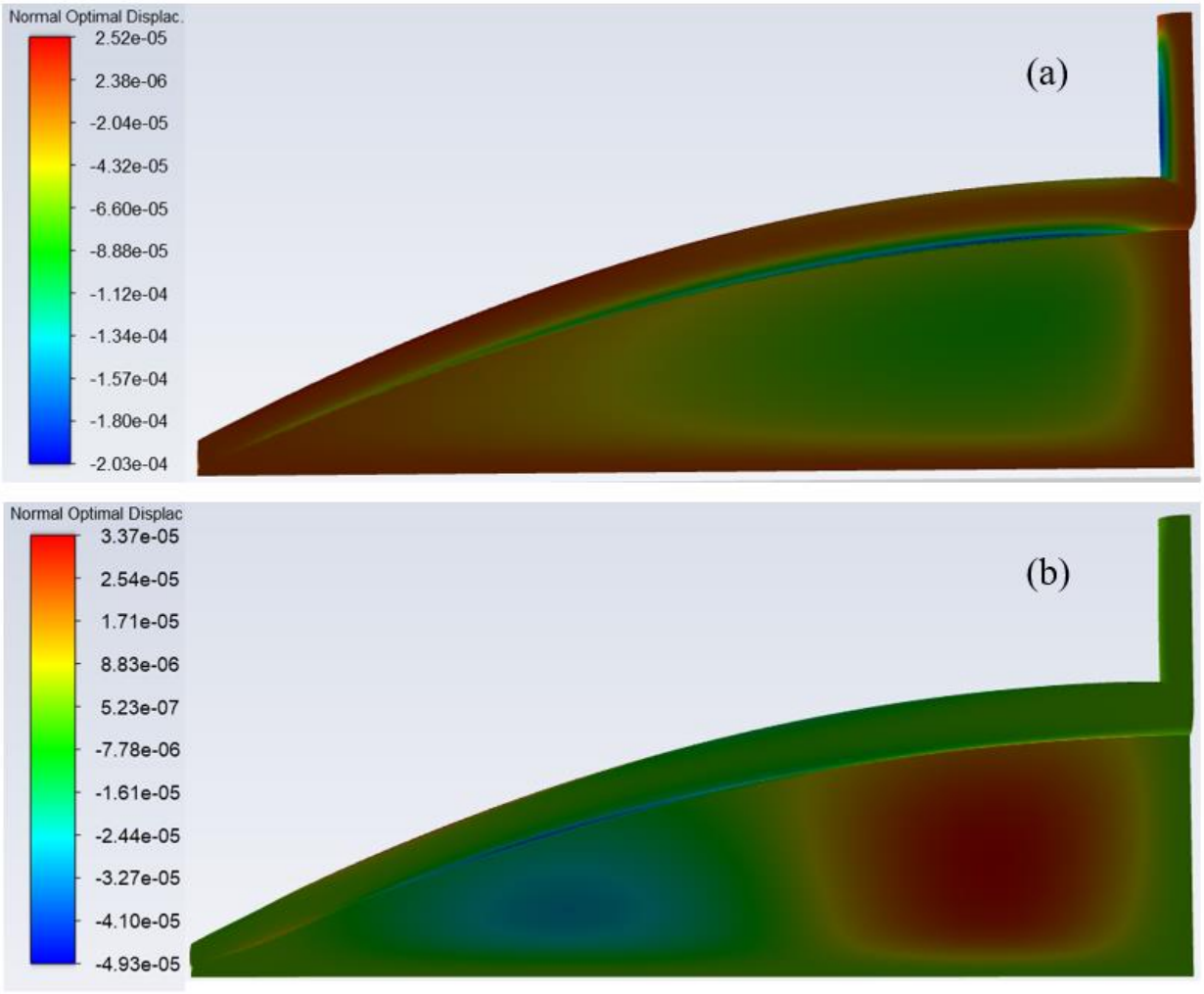

Figure 11: Die Fluid Body Displacement for (a) Observable: pressure drop and (b) Observable: mass-flux-variance Adjoint Optimization

5.1.8 Comparison of Residence Time

The residence time for the polymer melt for two material laws is shown in Figure 5.12. The residence time comparison for two rheological models, Power law and Carreau-Yasuda law, is shown in Figure 5.12. It can be observed that although the residence time distribution in the die while using the Power law is more uniform than while using the Carreau-Yasuda law, the residence time at the edge of the die is higher in the Power law melt than in the Carreau-Yasuda law melt. The maximum residence time at the edge of the die for Power-law is 1.81 seconds, while that for Carreau-Yasuda law is 2.29 seconds.

Optimizing the die using two observables, Pressure-drop and mass-flux-variance shows variation in the residence time as shown in

Figure 5.12; it is observed that the residence time distribution is non-uniform and very high up to 2.86 seconds towards the edge of the die when the Pressure drop is used as an observable for optimization but is more uniform and has a maximum residence time of 1.67 seconds at the edge of the die.

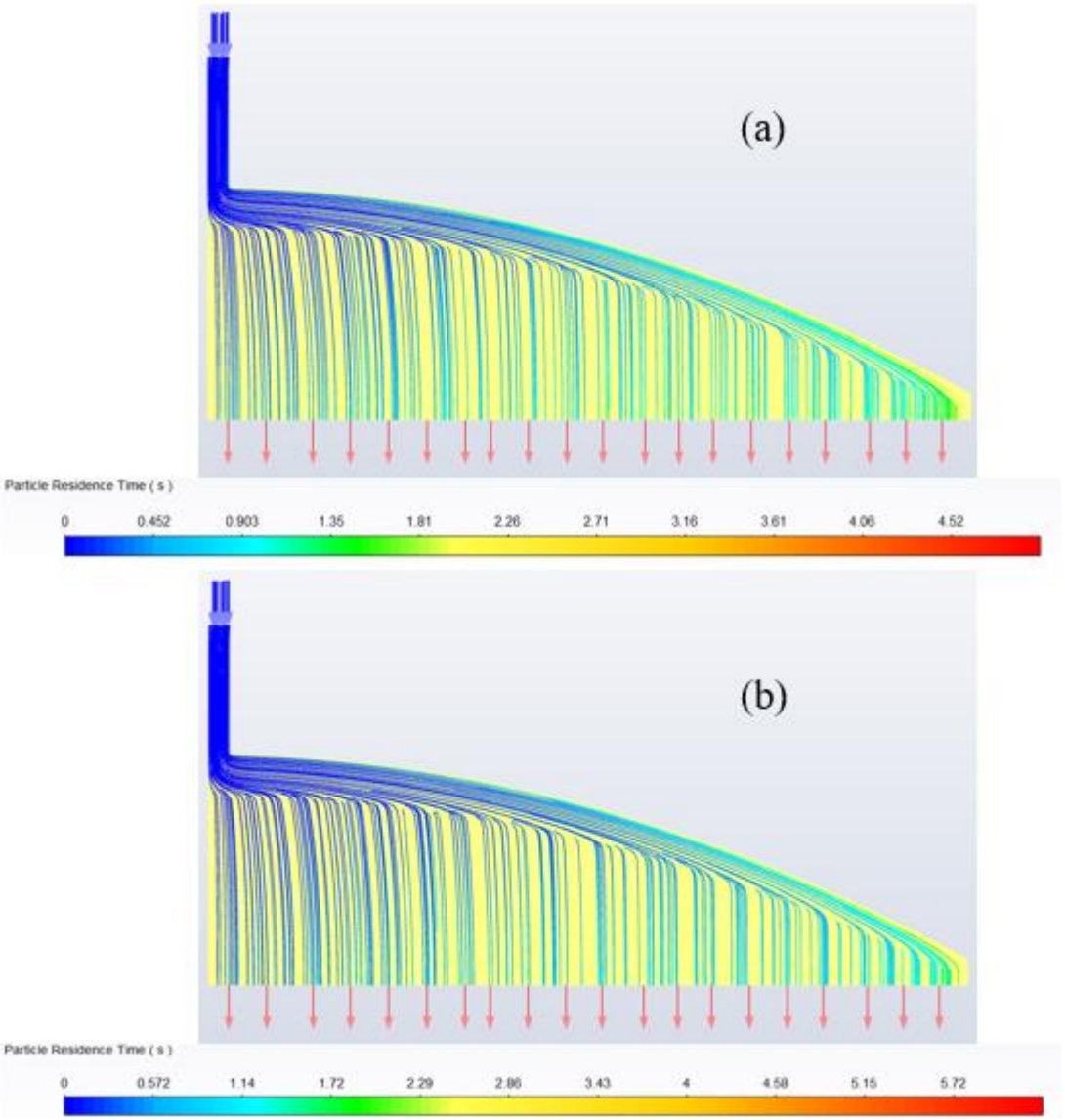

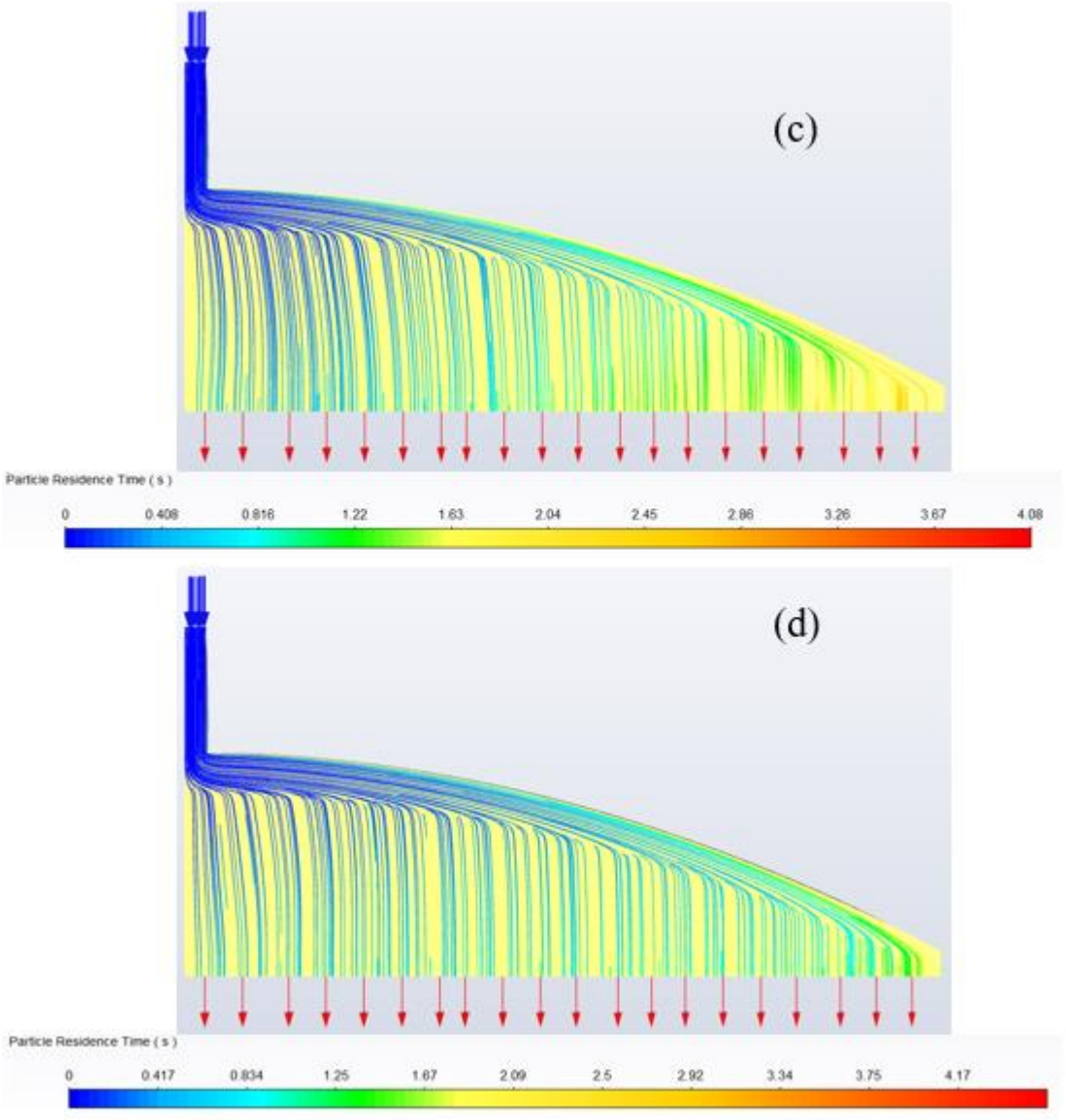

Figure 5.12: Residence Time for (a) Power Law (b) Carreau-Yasuda Law (c) Observable: Pressure drop (d) Observable: Mass-Flux-Variance

5.2 Concluding Remarks

Two primary considerations are put in place when designing a die for extrusion purposes: uniform velocity distribution at the die exit and minimal pressure loss between the inlet and outlet. This is because the quality of products and the power consumption by the die are influenced by uniform velocity distribution at the die exit and minimal pressure loss, respectively. Also, a die, which performs very well when used to extrude a particular material, may give different results when it is used to extrude a different material. As shown in Figure 5.1, the die exit velocity distribution is more uniform when a power law material is used than when a Carreau-Yasuda material is used.

One possible way to enhance die performance is by maintaining uniform velocity distribution and minimal pressure drop irrespective of the material used, such as optimizing the die using the adjoint method. By computing gradients irrespective of the number of design variables present, the adjoint method can quickly and effectively optimize various engineering shape designs for optimal performance.

This study used two observables to optimize the die: pressure drop and mass-flux-variance. The first five iterations were performed for the pressure drop, which reduced the Pressure from 3990651.3 Pa to 3350517.8 Pa (16.04% reduction). In comparison, 24 iterations were performed using the mass-flux-variance, and this reduces the mass-flux-variance from 0.025834378 kg/m-2s-1 to 0.011228295 kg/m-2s-1 (56.54% reduction). Also, the residence time distribution was reduced from 2.29 seconds to 1.67 seconds after optimization.

Future Work

Currently, no work experimentally validates the FSI of the melt flow through the coat-hanger die. Hence, one of the future works is to carry out experimental validation of the distribution of pressure, velocity, and shear stress in the die.

Secondly, the pressure drop, and mass-flux variation must be combined as a single observable to optimize the die for minimal pressure drop and uniform exit velocity. This will also be considered in the future.

Lastly, after optimization, the exported STL file needs to be studied to compare the direct results obtained from optimization simulation and the results obtained from performing direct simulation on the optimized geometry.

References

[1] P. F. Antonietti Politecnico di Milano, N. Aiman Fadel, M. Verani Politecnico di Milano, P. F. Antonietti, and M. Verani, "Modelling and numerical simulation of the polymeric extrusion process in textile products," pp. 1–13, doi: 10.1685/2010CAIM496.

[2] O. Yilmaz and K. Kirkkopru, "Design of a process material independent conical coat-hanger die by analytical approach," *Fibers and Polymers*, vol. 16, no. 9, pp. 1955–1963, 2015, doi: 10.1007/s12221-015-5292-z.

[3] N. Lebaal, F. Schmidt, and S. Puissant, "Optimizations of coat-hanger die, using constraint optimization algorithm and taguchi method," *AIP Conf Proc*, vol. 908, pp. 537–544, 2007, doi: 10.1063/1.2740866.

[4] W. Han and X. Wang, "Multi-objective optimization of the coat-hanger die for melt-blowing process," *Fibers and Polymers*, vol. 13, no. 5, pp. 626–631, May 2012, doi: 10.1007/s12221-012-0626-6.

[5] O. Yilmaz and K. Kirkkopru, "Design of a process material independent conical coat-hanger die by analytical approach," *Fibers and Polymers*, vol. 16, no. 9, pp. 1955–1963, Sep. 2015, doi: 10.1007/s12221-015-5292-z.

[6] W. Han and X. Wang, "Optimal geometry design of the coat-hanger die with uniform outlet velocity and minimal residence time," *J Appl Polym Sci*, vol. 123, no. 4, pp. 2511–2516, Feb. 2012, doi: 10.1002/APP.34827.

[7] R. Sander and J. F. T. Pittman, "Simulation of slit dies in operation including the interaction between melt pressure and die deflection," *Polym Eng Sci*, vol. 36, no. 15, pp. 1972–1989, 1996, doi: 10.1002/pen.10593.

[8] W. A. Gifford, "Three-dimensional analysis of coextrusion in a single manifold flat die," *Polym Eng Sci*, vol. 40, no. 9, pp. 2095–2100, 2000, doi: 10.1002/pen.11341.

[9] H. H. Winter and H. G. Fritz, "Design of dies for the extrusion of sheets and annular parisons: The distribution problem," *Polym Eng Sci*, vol. 26, no. 8, pp. 543–553, 1986, doi: 10.1002/pen.760260805.

[10] D. Igali, A. Perveen, D. Zhang, and D. Wei, "Shear rate coat-hanger die using casson viscosity model," *Processes*, vol. 8, no. 12, pp. 1–17, 2020, doi: 10.3390/pr8121524.

[11] M. Pini, G. Persico, D. Pasquale, and S. Rebay, "Adjoint method for shape optimization in real-gas flow applications," *J Eng Gas Turbine Power*, vol. 137, no. 3, pp. 1–14, 2015, doi: 10.1115/1.4028495.

[12] M. A. Aiman, N. A. Ramlee, M. A. Mohamad Azmi, and T. N. A. Tuan Sabri, "Preparation, thermal degradation, and rheology studies for polylactic acid (PLA) and palm stearin (PS) blend: A review," *Mater Today Proc*, vol. 63, pp. S222–S230, Jan. 2022, doi: 10.1016/j.matpr.2022.02.420.

[13] S. Maiti, M. R. Islam, M. A. Uddin, S. Afroj, S. J. Eichhorn, and N. Karim, "Sustainable Fiber-Reinforced Composites: A Review," *Advanced Sustainable Systems*, vol. 6, no. 11. John Wiley and Sons Inc, Nov. 01, 2022. doi: 10.1002/adsu.202200258.

[14] J. R. Wagner, E. M. Mount, and H. F. Giles, *Extrusion: The Definitive Processing Guide and Handbook: Second Edition*. 2013. doi: 10.1016/C2010-0-67040-4.

[15] C. Rauwendaal, *Polymer extrusion*.

[16] "Plastic extrusion - Wikipedia." Accessed: Nov. 15, 2023. [Online]. Available: https://en.wikipedia.org/wiki/Plastic_extrusion

[17] J. Vlachopoulos and N. D. Polychronopoulos, "RHEOLOGY AND TECHNOLOGY OF POLYMER EXTRUSION First Edition." [Online]. Available: www.polydynamics.com

[18] S. K. R. Manas Chanda, *Industrial Polymers, Specialty Polymers, and Their Applications*. 2009.
[19] G. Wypych, *Handbook of Polymers - George Wypych - Google Books*. 2012. [Online]. Available: https://books.google.com/books?hl=en&lr=&id=aedxCQAAQBAJ&oi=fnd&pg=PP1&dq=vinyl+acetate+polymerization&ots=h0M-MLNCUN&sig=Z_9buyuKcjTEVOO6iWZ6-1Np4VY#v=onepage&q=vinyl acetate polymerization&f=false
[20] D. G. Baird, "Polymer Processing," 2001.
[21] C. Hopmann and W. Michaeli, *Extrusion Dies for Plastics and Rubber*. 2016. doi: 10.3139/9781569906248.fm.
[22] Y. Matsubara, "Geometry Design of a Coat-Hanger Die with Uniform Flow Rate and Residence Time Across the Die Width."
[23] Y. Matsubara, "Residence Time Distribution of Polymer Melts in the Linearly Tapered Coat-Hanger Die."
[24] H. H. Winter and H. G. Fritz, "Design of dies for the extrusion of sheets and annular parisons: The distribution problem," *Polym Eng Sci*, vol. 26, no. 8, pp. 543–553, 1986, doi: 10.1002/pen.760260805.
[25] T.-J. Liu, C.-N. Hong, and K.-C. Chen, "Computer-Aided Analysis of a Linearly Tapered Coat-Hanger Die."
[26] K.-Y. Lee and T.-J. Liu, "Design and Analysis of a Dual-Cavity Coat-Hanger Die-ner cavity."
[27] T.-J. Liu, L.-D. Liu, and C. Shan, "A Unified Lubrication Approach for the Design of a Coat-Hanger Die."
[28] S. Yeon Na and D. Hyun Kim, "THREE-DIMENSIONAL MODELLING OF NON-NEWTONIAN FLUID FLOW IN A COAT-HANGER DIE," 1995.
[29] Y. Huang, C. R. Gentle, and J. B. Hull, "A comprehensive 3-D analysis of polymer melt flow in slit extrusion dies," *Advances in Polymer Technology*, vol. 23, no. 2, pp. 111–124, Jun. 2004, doi: 10.1002/adv.20002.
[30] C. Chen, P. Jen, and F. S. La1, "Optimization of the Coat-hanger Manifold via Computer Simulation and an Orthogonal Array Method."
[31] A. Razeghiyadaki, D. Zhang, D. Wei, and A. Perveen, "Optimization of polymer extrusion die based on response surface method," *Processes*, vol. 8, no. 9, Sep. 2020, doi: 10.3390/pr8091043.
[32] A. Razeghiyadaki, D. Wei, A. Perveen, and D. Zhang, "A multi-rheology design method of sheeting polymer extrusion dies based on flow network and the winter-fritz design equation," *Polymers (Basel)*, vol. 13, no. 12, Jun. 2021, doi: 10.3390/polym13121924.
[33] N. Lebaal, F. Schmidt, S. Puissant, N. Lebaal, F. Schmidt, and S. Puissant, "Optimization of 3D die extrusion using response surface method O ptimization of 3D die extrusion using response surface method." [Online]. Available: https://hal.science/hal-01788407
[34] N. Lebaal, F. Schmidt, and S. Puissant, "Design and optimization of three-dimensional extrusion dies, using constraint optimization algorithm," *Finite Elements in Analysis and Design*, vol. 45, no. 5, pp. 333–340, Apr. 2009, doi: 10.1016/j.finel.2008.10.008.
[35] N. Lebaal, F. Schmidt, and S. Puissant, "Optimisation of extrusion flat die design and die wall temperature distribution, using Kriging and response surface method," *International Journal of Materials and Product Technology*, vol. 38, no. 2–3, pp. 307–322, 2010, doi: 10.1504/IJMPT.2010.032107.

[36] N. Lebaal, S. Puissant, F. M. Schmidt, and D. Schläfli, “An optimization method with experimental validation for the design of extrusion wire coating dies for a range of different materials and operating conditions,” *Polym Eng Sci*, vol. 52, no. 12, pp. 2675–2687, Dec. 2012, doi: 10.1002/pen.23203.

[37] N. Lebaal, F. Schmidt, and S. Puissant, “Optimizations of coat-hanger die, using constraint optimization algorithm and taguchi method,” *AIP Conf Proc*, vol. 908, pp. 537–544, 2007, doi: 10.1063/1.2740866.

[38] W. Han and X. Wang, “Optimal geometry design of the coat-hanger die used for melt blown nonwoven processing,” in *Advanced Materials Research*, 2011, pp. 444–448. doi: 10.4028/www.scientific.net/AMR.331.444.

[39] J. P. Heners, L. Radtke, M. Hinze, and A. Düster, “Adjoint shape optimization for fluid–structure interaction of ducted flows,” *Comput Mech*, vol. 61, no. 3, pp. 259–276, 2018, doi: 10.1007/s00466-017-1465-5.

[40] A. Razeghiyadaki, D. Zhang, D. Wei, and A. Perveen, “Optimization of polymer extrusion die based on response surface method,” *Processes*, vol. 8, no. 9, 2020, doi: 10.3390/pr8091043.

[41] W. A. Gifford, “The effect of wall slip on the performance of flat extrusion dies,” *Polym Eng Sci*, vol. 41, no. 11, pp. 1886–1892, Nov. 2001, doi: 10.1002/pen.10885.

[42] D. Igali, A. Perveen, D. Zhang, and D. Wei, “Shear rate coat-hanger die using casson viscosity model,” *Processes*, vol. 8, no. 12, pp. 1–17, Dec. 2020, doi: 10.3390/pr8121524.

[43] M. Pini, G. Persico, D. Pasquale, and S. Rebay, “Adjoint method for shape optimization in real-gas flow applications,” *J Eng Gas Turbine Power*, vol. 137, no. 3, pp. 1–13, 2015, doi: 10.1115/1.4028495.

[44] D. E. Smith and Q. Wang, “Optimization-based design of polymer sheeting dies using generalized newtonian fluid models,” *Polym Eng Sci*, vol. 45, no. 7, pp. 953–965, Jul. 2005, doi: 10.1002/PEN.20347.

[45] D. E. Smith and Q. Wang, “Optimization-based design of polymer sheeting dies using generalized newtonian fluid models,” *Polym Eng Sci*, vol. 45, no. 7, pp. 953–965, Jul. 2005, doi: 10.1002/pen.20347.

[46] R. Sander and J. F. T. Pittman, “Simulation of slit dies in operation including the interaction between melt pressure and die deflection,” *Polym Eng Sci*, vol. 36, no. 15, pp. 1972–1989, 1996, doi: 10.1002/pen.10593.

Appendices

Appendice A

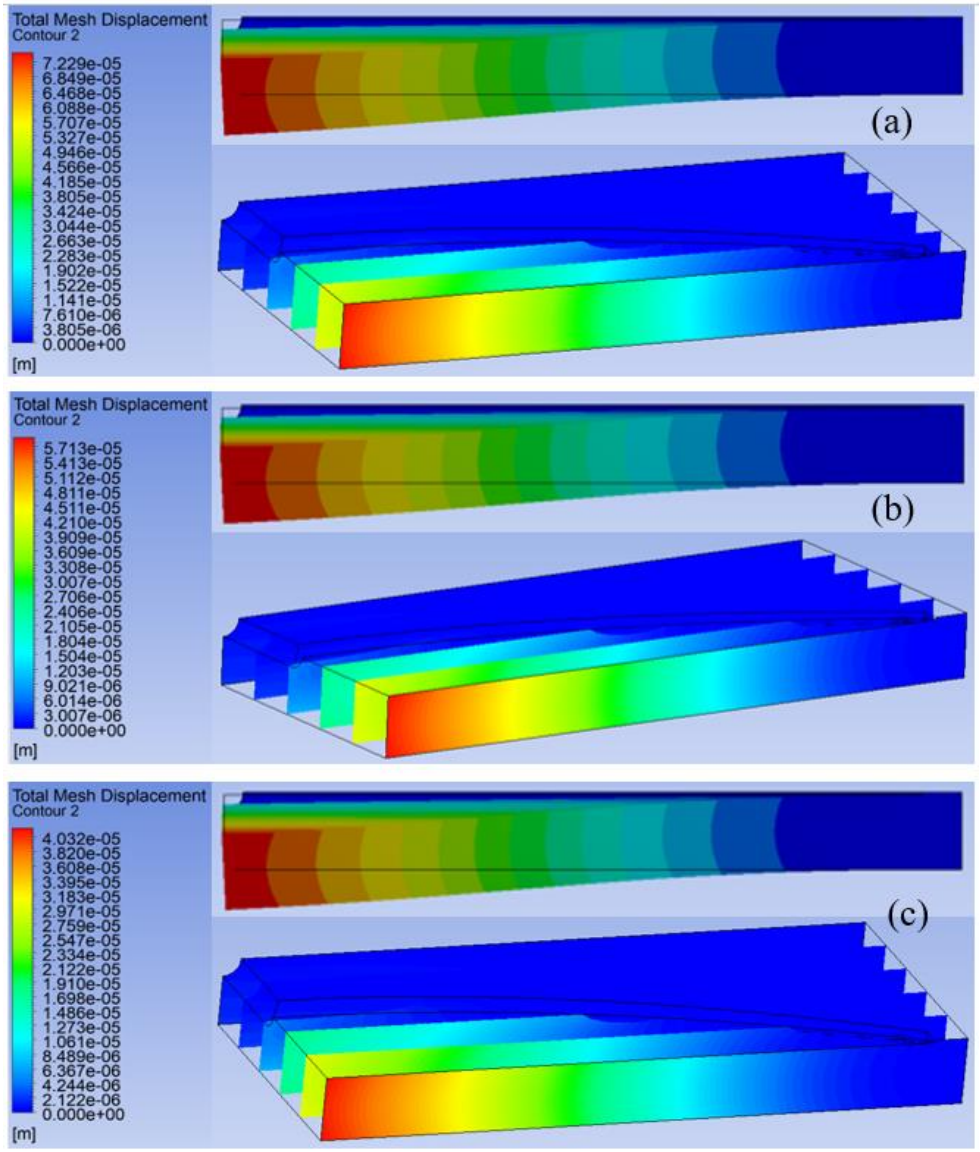

Figure A.1 Deflection at various Planes for (a) Power-law (b) Cross-law and (c) Carreau-Yasuda law

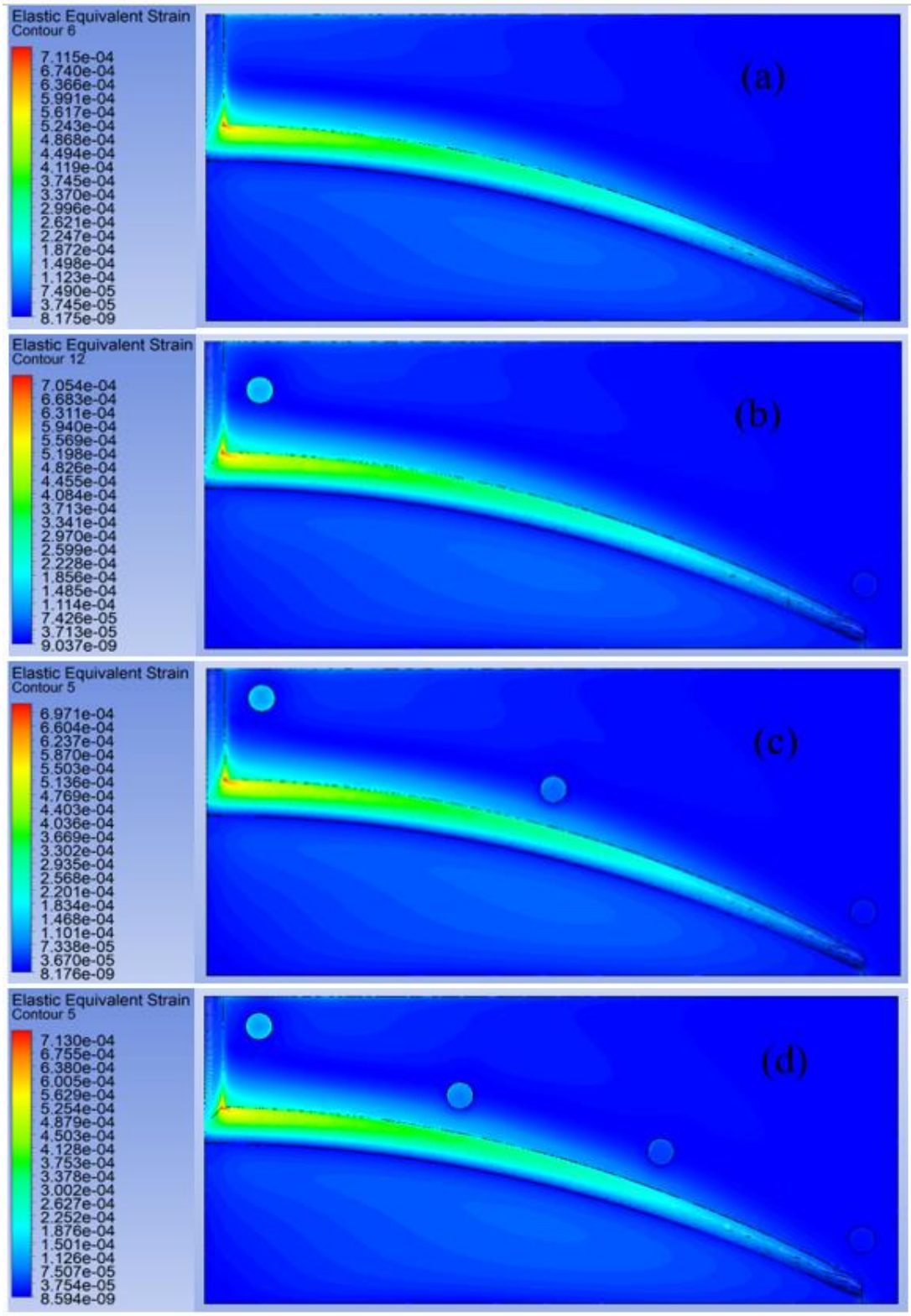

Figure A.2 Equivalent Strain at various Planes for (a) Power-law (b) Cross-law and (c) Carreau-Yasuda law

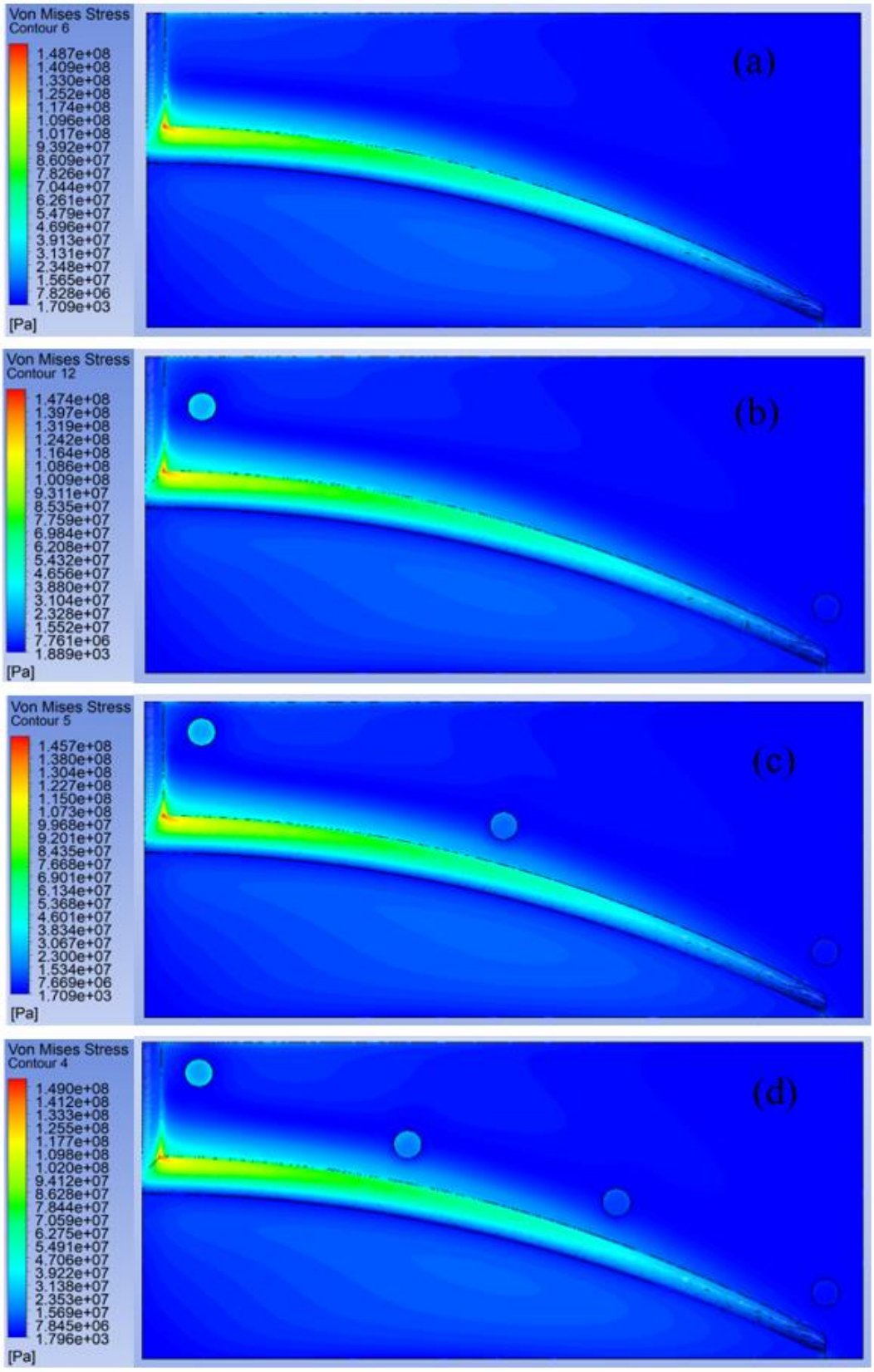

Figure A.3 Equivalent Stress at various Planes for (a) Power-law (b) Cross-law and (c) Carreau-Yasuda law

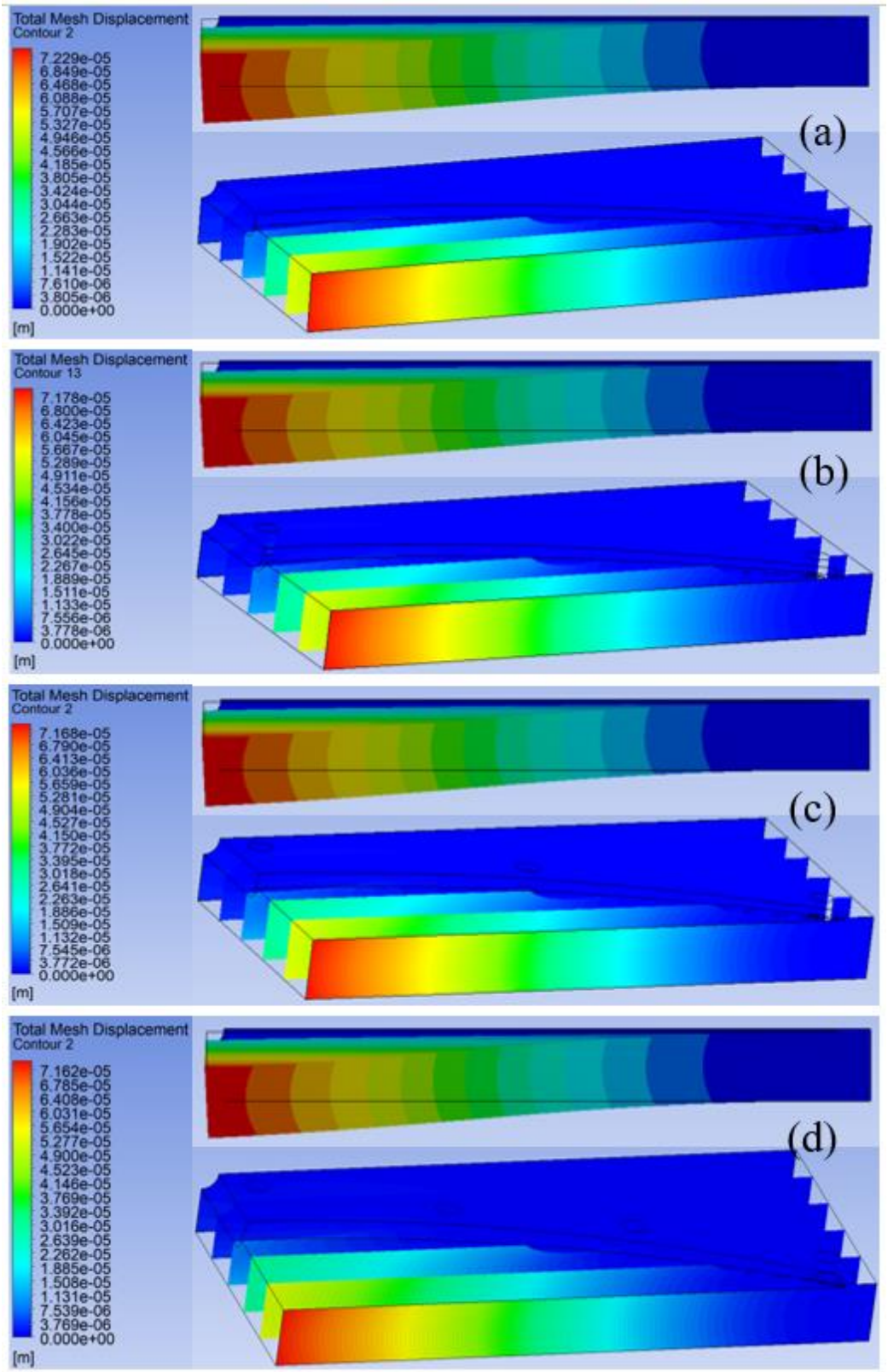

Figure A.4 Deflection for (a) 0 (b) 2 (c) 3 (d) 4 Supports

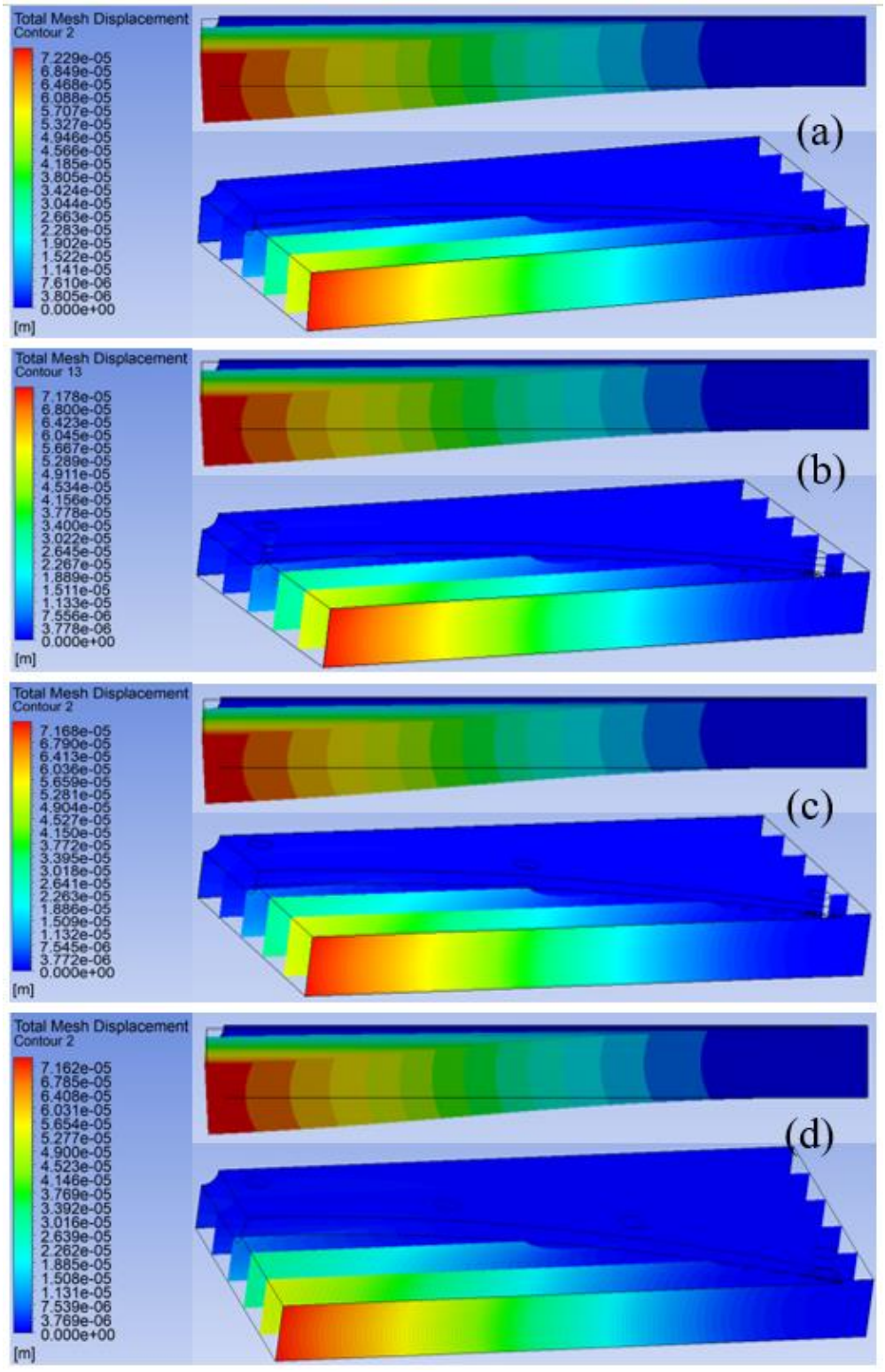

Figure A.5 Equivalent Strain for (a) 0 (b) 2 (c) 3 (d) 4 Supports

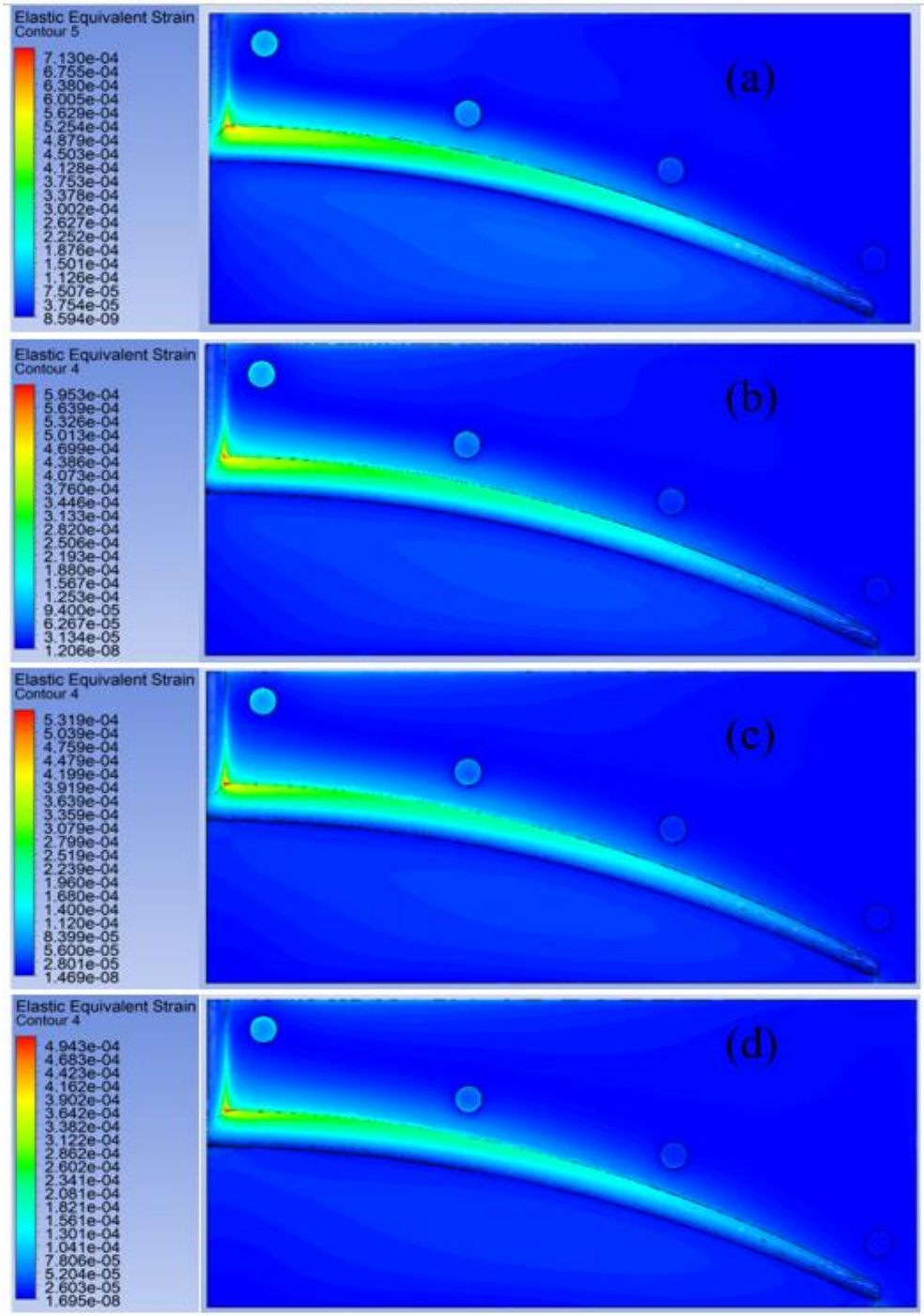
Elastic Equivalent Strain
Contour 5
7.130e-04
6.755e-04
6.380e-04
6.005e-04
5.629e-04
5.254e-04
4.879e-04
4.503e-04
4.128e-04
3.753e-04
3.378e-04
3.002e-04
2.627e-04
2.252e-04
1.876e-04
1.501e-04
1.126e-04
7.507e-05
3.754e-05
8.594e-09
(a)
Elastic Equivalent Strain
Contour 4
5.953e-04
5.639e-04
5.326e-04
5.013e-04
4.699e-04
4.386e-04
4.073e-04
3.760e-04
3.446e-04
3.133e-04
2.820e-04
2.506e-04
2.193e-04
1.880e-04
1.567e-04
1.253e-04
9.400e-05
6.267e-05
3.134e-05
1.206e-08
(b)
Elastic Equivalent Strain
Contour 4
5.319e-04
5.039e-04
4.759e-04
4.479e-04
4.199e-04
3.919e-04
3.639e-04
3.359e-04
3.079e-04
2.799e-04
2.519e-04
2.239e-04
1.960e-04
1.680e-04
1.400e-04
1.120e-04
8.399e-05
5.600e-05
2.801e-05
1.469e-08
(c)
Elastic Equivalent Strain
Contour 4
4.943e-04
4.683e-04
4.423e-04
4.162e-04
3.902e-04
3.642e-04
3.382e-04
3.122e-04
2.862e-04
2.602e-04
2.341e-04
2.081e-04
1.821e-04
1.561e-04
1.301e-04
1.041e-04
7.806e-05
5.204e-05
2.603e-05
1.695e-08
(d)

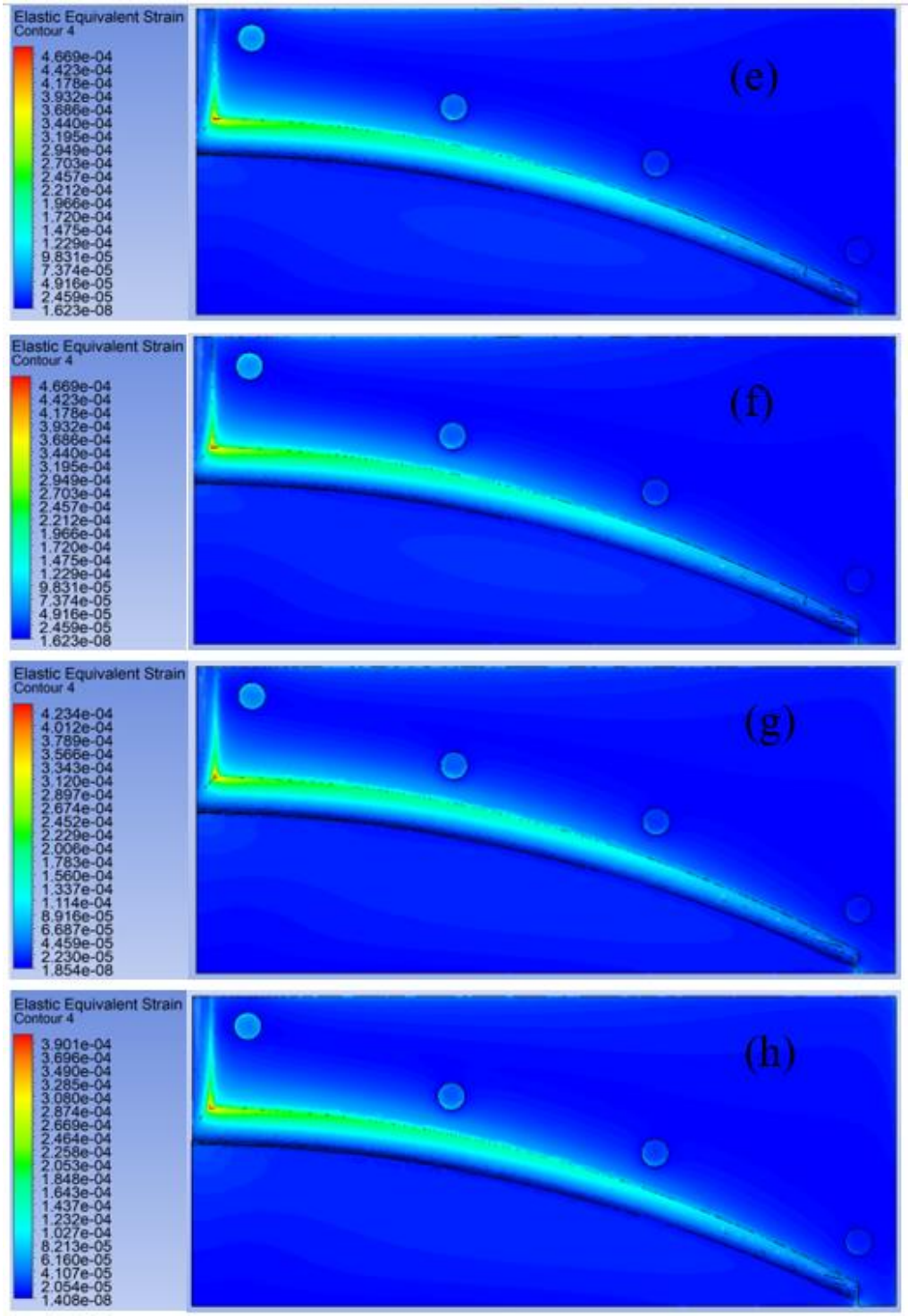

Figure A.6 Equivalent Elastic Strain for (a) 30mm (b) 40mm (c) 50mm (d) 60mm (e) 70mm (f) 80mm (g) 90mm and (h) 100mm Thickness

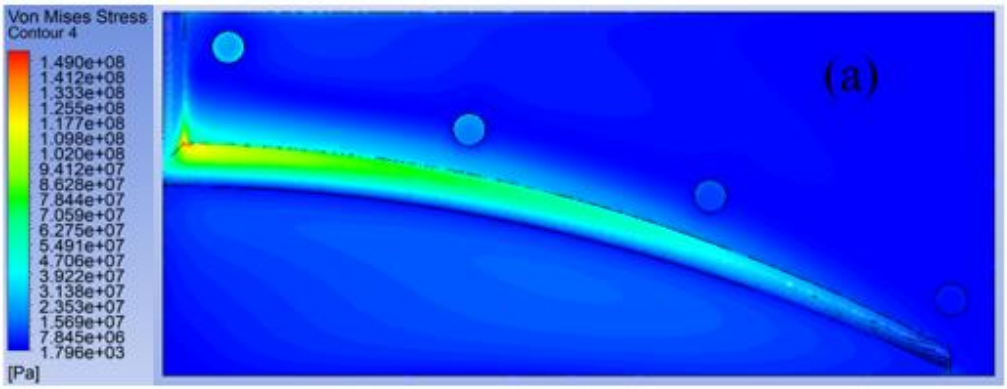
Von Mises Stress
Contour 4
1.490e+08
1.412e+08
1.333e+08
1.255e+08
1.177e+08
1.098e+08
1.020e+08
9.412e+07
8.628e+07
7.844e+07
7.059e+07
6.275e+07
5.491e+07
4.706e+07
3.922e+07
3.138e+07
2.353e+07
1.569e+07
7.845e+06
1.796e+03
[Pa]
(a)

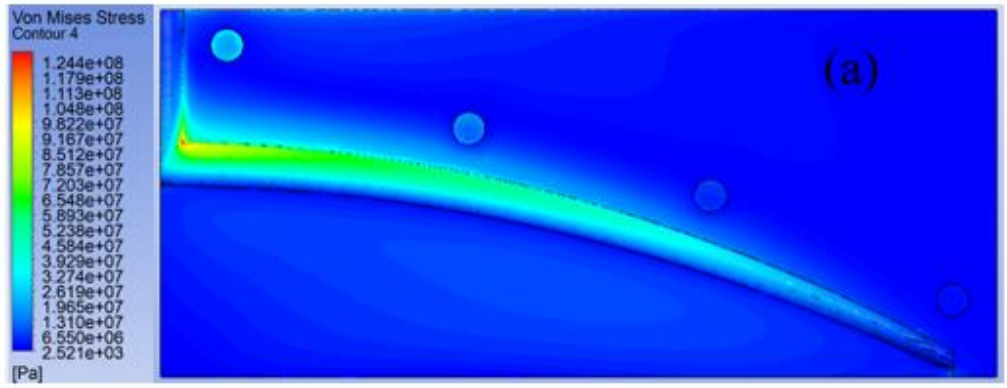
Von Mises Stress
Contour 4
1.244e+08
1.179e+08
1.113e+08
1.048e+08
9.822e+07
9.167e+07
8.512e+07
7.857e+07
7.203e+07
6.548e+07
5.893e+07
5.238e+07
4.584e+07
3.929e+07
3.274e+07
2.619e+07
1.965e+07
1.310e+07
6.550e+06
2.521e+03
[Pa]
(a)

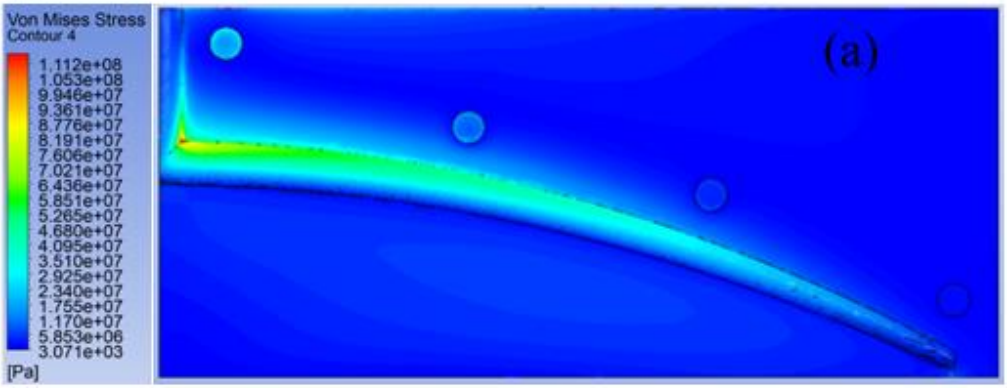
Von Mises Stress
Contour 4
1.112e+08
1.053e+08
9.946e+07
9.361e+07
8.776e+07
8.191e+07
7.606e+07
7.021e+07
6.436e+07
5.851e+07
5.265e+07
4.680e+07
4.095e+07
3.510e+07
2.925e+07
2.340e+07
1.755e+07
1.170e+07
5.853e+06
3.071e+03
[Pa]
(a)

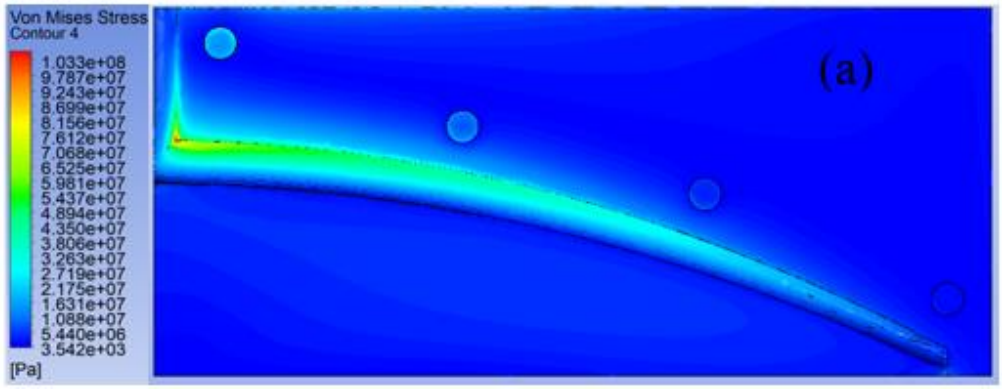
Von Mises Stress
Contour 4
1.033e+08
9.787e+07
9.243e+07
8.699e+07
8.156e+07
7.612e+07
7.068e+07
6.525e+07
5.981e+07
5.437e+07
4.894e+07
4.350e+07
3.806e+07
3.263e+07
2.719e+07
2.175e+07
1.631e+07
1.088e+07
5.440e+06
3.542e+03
[Pa]
(a)

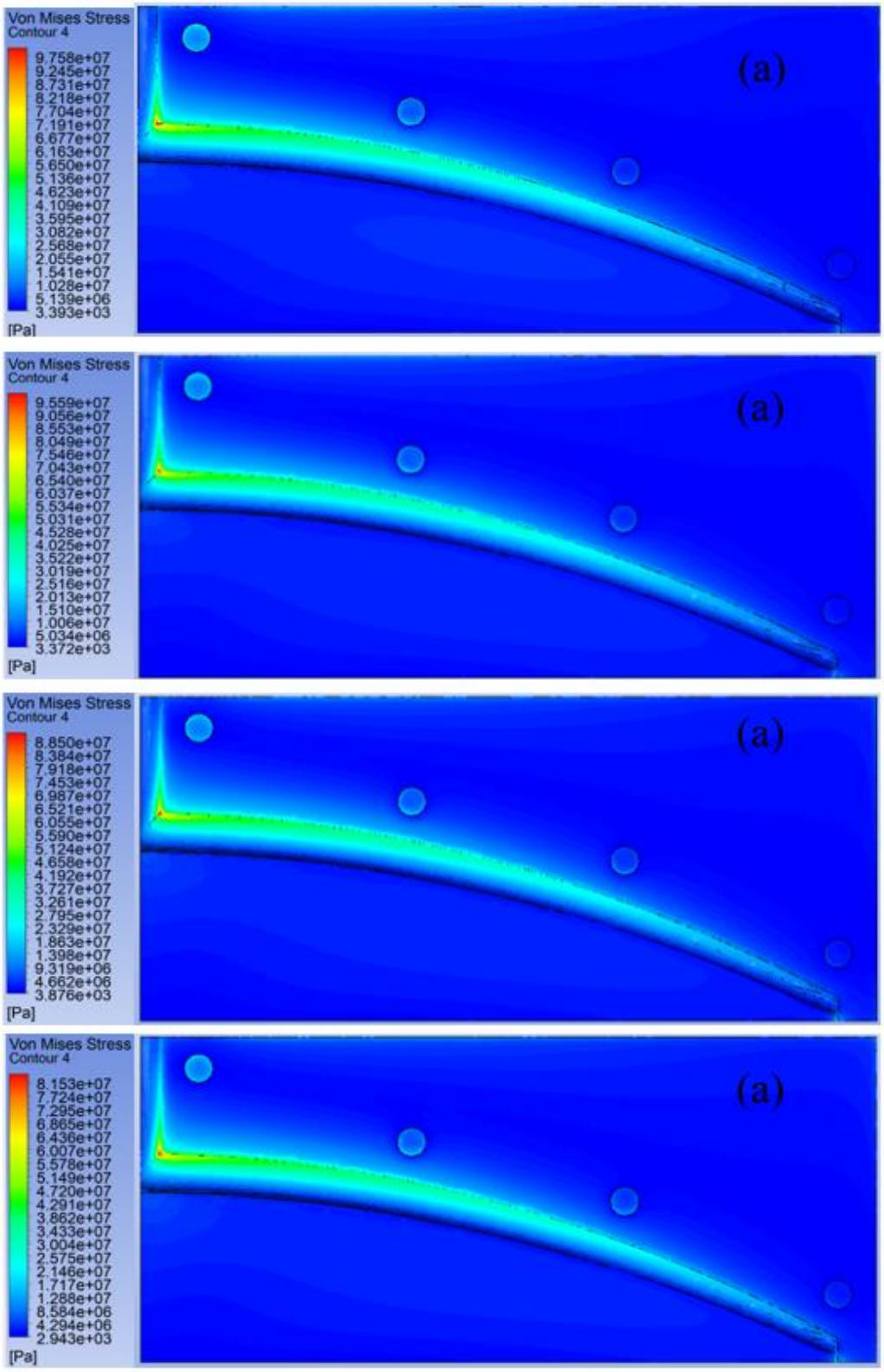

Figure A.7 Equivalent Elastic Stress for (a) 30mm (b) 40mm (c) 50mm (d) 60mm (e) 70mm (f) 80mm (g) 90mm and (h) 100mm Thickness

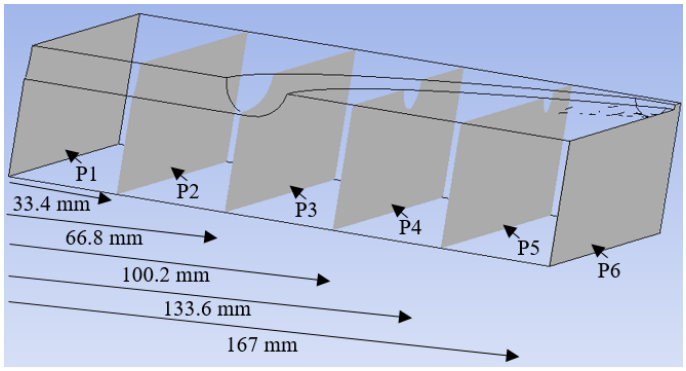

Figure A.8: Isometric view of various planes (P1, P2, P3, P4, P5 and P6)) and their distances from the inlet along Z-axis.

Table A.1 Deflection, Equivalent Strain and Stress for Different Material Law

S/No	**Material Law**	**Deflection (µm)**			**Stress (MPa)**		**Strain x 10^{-5}**	
		Max.	**Min.**	**Avg.**	**Max.**	**Min.**	**Max.**	**Min.**
1.	Power Law	74.58	0	9.34	153.34	0.00171	73.40	0.00082
2.	Cross Law	58.94	0	7.45	120.62	0.00141	57.71	0.00068
3.	Carreau-Yasuda Law	41.60	0	5.20	85.44	0.00095	40.88	0.00045

Table A.2 Deflection, Equivalent Strain and Stress for Different Supports

S/No.	**Supports**	**Deflection (µm)**			**Stress (MPa)**		**Strain x 10^{-5}**	
		Max.	**Min.**	**Avg.**	**Max.**	**Min.**	**Max.**	**Min.**
1.	0	74.58	0	9.34	153.34	0.00171	73.40	0.00082
2.	2	74.05	0	9.26	152.08	0.00189	72.77	0.00090
3.	3	73.94	0	9.25	150.29	0.00171	71.91	0.00082
4.	4	73.88	0	9.24	153.73	0.00180	73.56	0.00086

Table A.3 Deflection, Equivalent Strain and Stress for Different Thickness

S/No.	Thickness (mm)	Deflection (µm)			Stress (MPa)		Strain x 10^{-5}	
		Max.	Min.	Avg.	Max.	Min.	Max.	Min.
1.	30	73.88	0	9.24	153.73	0.00180	73.56	0.000860
2.	40	44.59	0	6.09	128.34	0.00257	61.41	0.000012
3.	50	31.69	0	4.74	114.67	0.00307	54.86	0.000015
4.	60	25.01	0	4.09	106.57	0.00354	50.99	0.000017
5.	70	21.08	0	3.74	100.67	0.00339	48.16	0.000016
6.	80	18.59	0	3.56	98.61	0.00337	47.18	0.000016
7.	90	16.81	0	3.46	91.29	0.00388	43.68	0.000019
8.	100	15.51	0	3.41	84.10	0.00294	40.24	0.000014

Appendice B

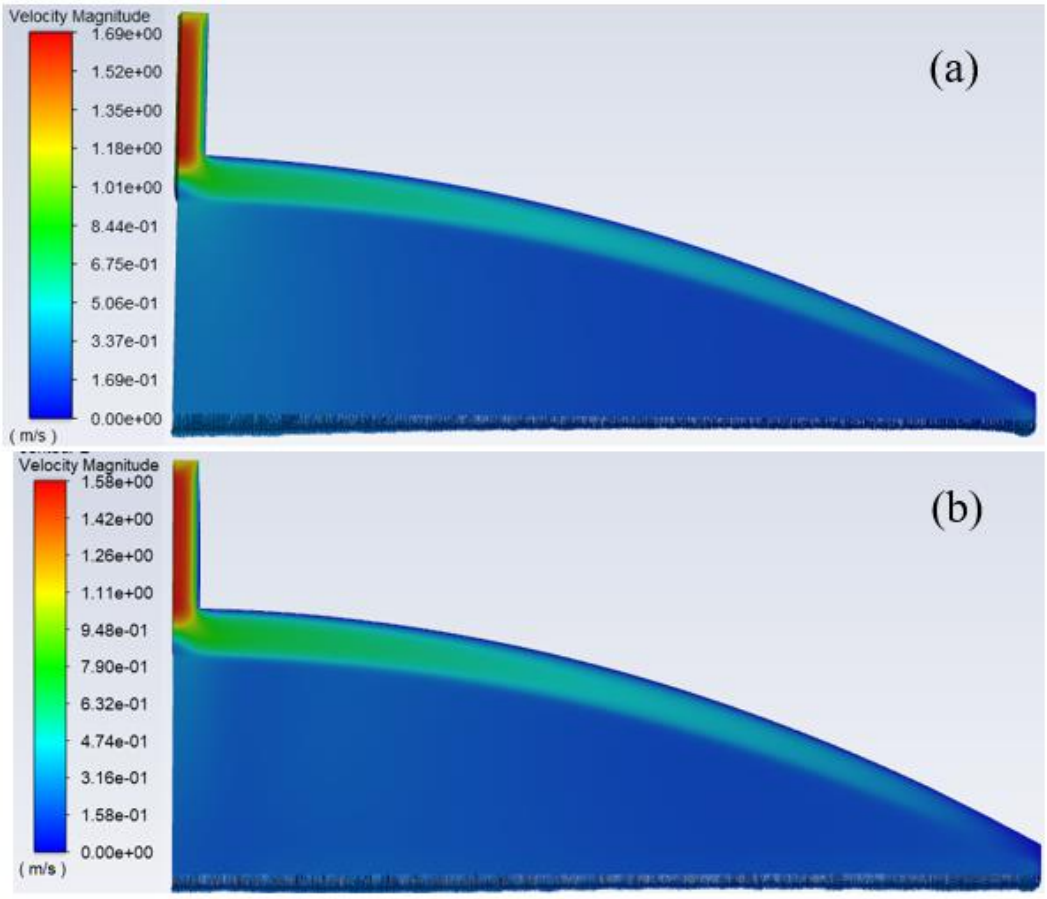

Figure B.1 Velocity Vector at Die Outlet for (a) Power-law and (b) Carreau-Yasuda law

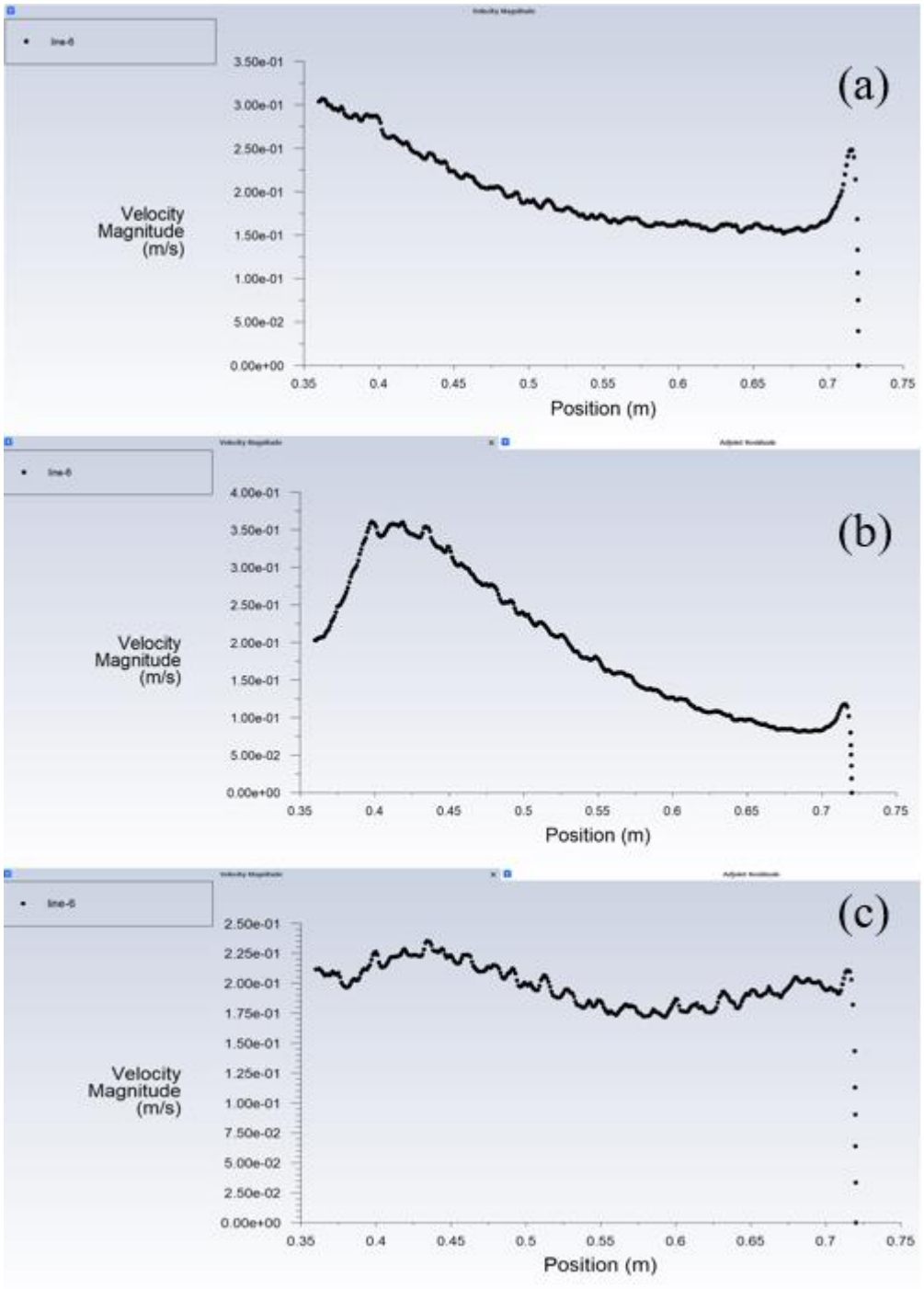

Figure B.2 Velocity Distribution at the Die Exit for (a) Initial (b) Observabele: pressure drop and (c) Observable: mass-flux-variance Die Design

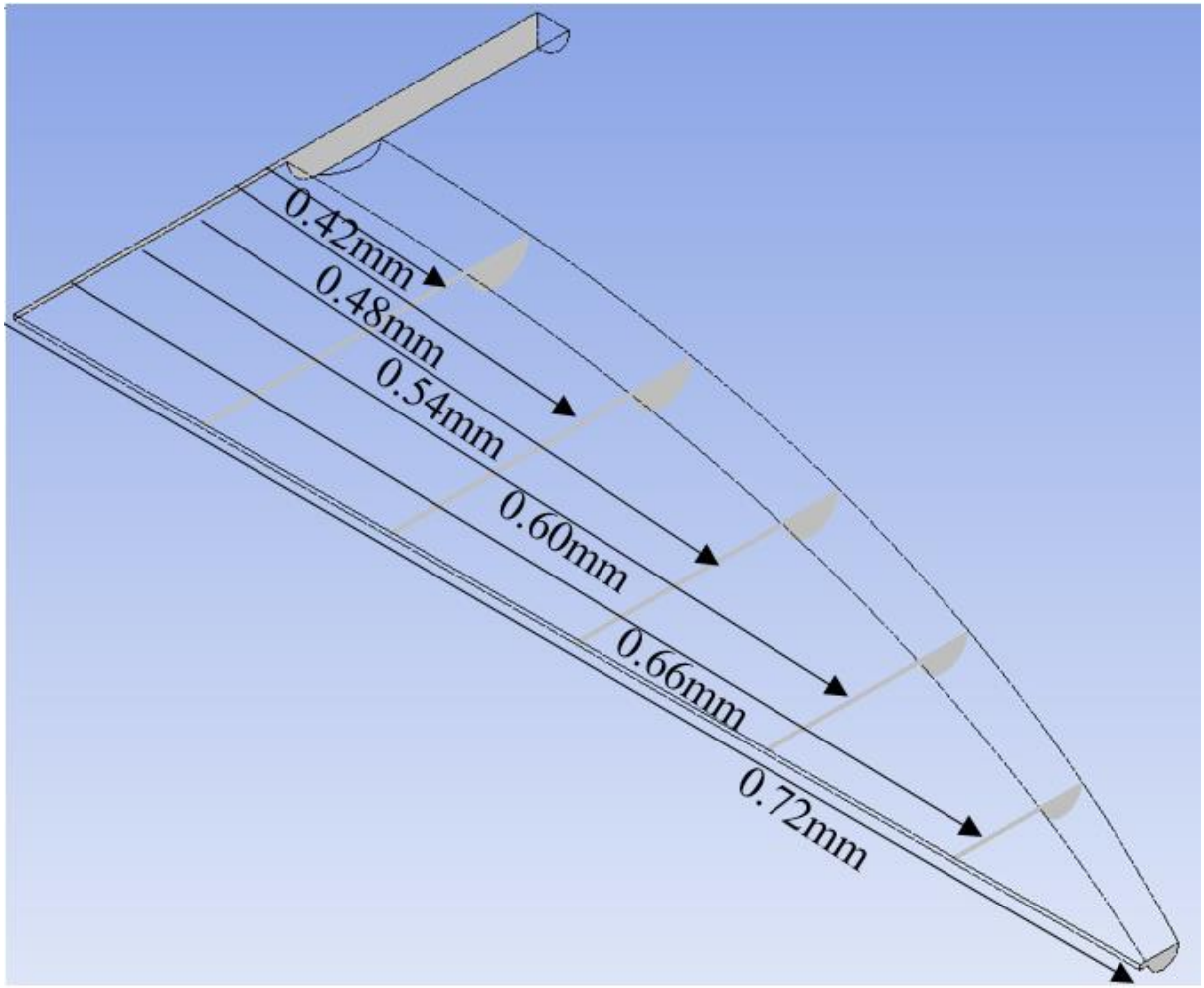

Figure B.3 Distances of Planes from Die Center

```
(define start_loop 1)
(define end_loop 5)
(define x start_loop)
(define max-iter-adjoint 150)

(do ((x start_loop (+ x 1))) ((> x end_loop))


    (display x)


    (ti-menu-load-string (format #f "/adjoint/run/iterate ~a \n" max-iter-adjoint))


    (ti-menu-load-string "/adjoint/design-tool/design-change/calculate-design-change \n")
    (ti-menu-load-string "/adjoint/design-tool/design-change/modify-mesh \n")


    (ti-menu-load-string "solve iterate,")


    (ti-menu-load-string "/adjoint/observable/select \"pressure-drop\" no \n")
    (ti-menu-load-string "/adjoint/observable/write yes observables.txt yes \n")
    (ti-menu-load-string "/adjoint/observable/select \"pressure-drop\" no \n")


)


```

Figure B.4 Scheme Program for Observable: Pressure drop

```
(define start_loop 1)
(define end_loop 20)
(define x start_loop)
(define max-iter-adjoint 150)

(do ((x start_loop (+ x 1))) ((> x end_loop))


    (display x)


    (ti-menu-load-string (format #f "/adjoint/run/iterate ~a \n" max-iter-adjoint))


    (ti-menu-load-string "/adjoint/design-tool/design-change/calculate-design-change \n")
    (ti-menu-load-string "/adjoint/design-tool/design-change/modify-mesh \n")


    (ti-menu-load-string "solve iterate,")


    (ti-menu-load-string "/adjoint/observable/select \"mass-flux-variance\" no \n")
    (ti-menu-load-string "/adjoint/observable/write yes observables.txt yes \n")
    (ti-menu-load-string "/adjoint/observable/select \"mass-flux-variance\" no \n")


)
```

Figure B.5 Scheme Program for Observable: mass-flux-variance

Table B.1 Pressure and Wall shear stress at Different Planes for Various Die Designs

S/no.	Plane	Initial Die		Observable: Pressure drop		Observable: mass-flux-variance	
	Distance from Die Center (mm)	Pressure (Pa)	Wall Shear Stress (Pa)	Pressure (Pa)	Wall Shear Stress (Pa)	Pressure (Pa)	Wall Shear Stress (Pa)
1.	0.36	4212840	64628.95	3574390	64021.05	3912500	64191.9
2.	0.42	2873860	42843.2	2294810	44436.55	2623790	41359.8
3.	0.48	2436740	41083.05	1898520	40392.65	2204290	39687.75
4.	0.54	1988210	40956.7	1520850	36198.3	1786230	38881.55
5.	0.6	1484220	38840.6	1120110	31932.1	1321730	36948.45
6.	0.66	887481	37792	664386	29532.6	780711	36684.9
7.	0.72	261287	16399.36	97859	12436.405	244246	30613.73

Table B.2 Velocity at Different Planes for Various Die Designs

S/no.	Plane	Initial Die	Observable: Pressure drop	Observable: mass-flux-variance
	Distance from Die Center (mm)	**Velocity (m/s)**	**Velocity (m/s)**	**Velocity (m/s)**
1.	0.36	0.303605	0.201227	0.208467
2.	0.38	0.283666	0.260909	0.194331
3.	0.4	0.282653	0.361335	0.225221
4.	0.42	0.251737	0.355413	0.225071
5.	0.44	0.235181	0.329882	0.226931
6.	0.46	0.215121	0.297023	0.221439
7.	0.48	0.203122	0.271405	0.211609
8.	0.5	0.189958	0.236984	0.201016
9.	0.52	0.179688	0.207793	0.189253
10.	0.54	0.168429	0.177242	0.177906
11.	0.56	0.16298	0.156496	0.171732
12.	0.58	0.15952	0.138287	0.171987

13.	0.6	0.164614	0.128309	0.18688
14.	0.62	0.153977	0.106941	0.174017
15.	0.64	0.1555	0.0977136	0.179148
16.	0.66	0.155818	0.08954	0.190121
17.	0.68	0.157052	0.083753	0.203683
18.	0.7	0.166883	0.0818366	0.193154
19.	0.72	0.174198	0.0826463	0.148572